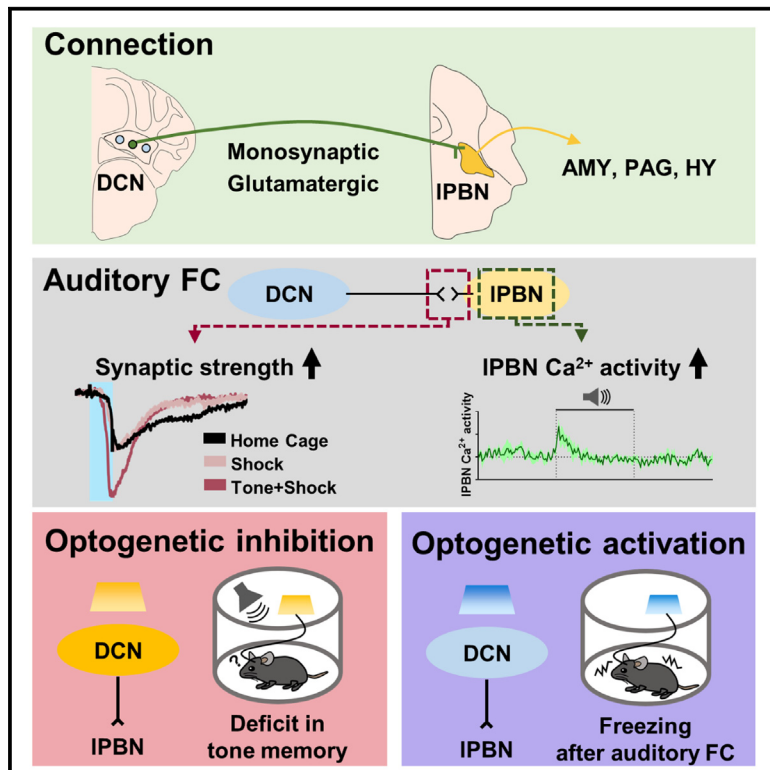


Cerebellar nuclei neurons projecting to the lateral parabrachial nucleus modulate classical fear conditioning

Graphical abstract



Authors

Kyoung-Doo Hwang, Jinhee Baek, Hyun-Hee Ryu, ..., Sun Yong Kim, Sang Jeong Kim, Yong-Seok Lee

Correspondence

sangjikim@snu.ac.kr (S.J.K.),
yongseok7@snu.ac.kr (Y.-S.L.)

In brief

Hwang et al. identify a cerebellar output pathway from deep cerebellar nuclei to the lateral parabrachial nucleus critical for auditory fear conditioning. Using a combination of techniques, including electrophysiology, optogenetic manipulations, and fiber photometry recordings, they show that this circuit carries information about conditioned auditory stimuli during classical fear conditioning.

Highlights

- Deep cerebellar nuclei (DCN) project to the lateral parabrachial nucleus (IPBN)
- $\text{DCN} \rightarrow \text{IPBN}$ neuron activation is necessary for auditory fear conditioning
- Auditory fear conditioning induces synaptic potentiation at DCN-PBN synapses



Article

Cerebellar nuclei neurons projecting to the lateral parabrachial nucleus modulate classical fear conditioning

Kyoung-Doo Hwang,^{1,2} Jinhee Baek,^{1,2} Hyun-Hee Ryu,^{1,3} Jaegeon Lee,^{1,2} Hyun Geun Shim,^{1,2} Sun Yong Kim,^{1,2} Sang Jeong Kim,^{1,2,3,4,*} and Yong-Seok Lee^{1,2,3,4,5,*}

¹Department of Physiology, Seoul National University College of Medicine, Seoul 03080, Republic of Korea

²Department of Biomedical Science, Seoul National University College of Medicine, Seoul 03080, Republic of Korea

³Neuroscience Research Institute, Seoul National University College of Medicine, Seoul 03080, Republic of Korea

⁴Wide River Institute of Immunology, Seoul National University, Hongcheon, Republic of Korea

⁵Lead contact

*Correspondence: sangjkim@snu.ac.kr (S.J.K.), yongseok7@snu.ac.kr (Y.-S.L.)

<https://doi.org/10.1016/j.celrep.2023.112291>

SUMMARY

Multiple brain regions are engaged in classical fear conditioning. Despite evidence for cerebellar involvement in fear conditioning, the mechanisms by which cerebellar outputs modulate fear learning and memory remain unclear. We identify a population of deep cerebellar nucleus (DCN) neurons with monosynaptic glutamatergic projections to the lateral parabrachial nucleus (IPBN) ($DCN \rightarrow^{IPBN}$ neurons) in mice. While optogenetic suppression of $DCN \rightarrow^{IPBN}$ neurons impairs auditory fear memory, activation of $DCN \rightarrow^{IPBN}$ neurons elicits freezing behavior only after auditory fear conditioning. Moreover, auditory fear conditioning potentiates DCN-IPBN synapses, and subsequently, auditory cue activates IPBN neurons after fear conditioning. Furthermore, DCN-IPBN neuron activation can replace the auditory cue but not footshock in fear conditioning. These findings demonstrate that cerebellar nuclei modulate auditory fear conditioning via transmitting conditioned stimuli signals to the IPBN. Collectively, our findings suggest that the DCN-IPBN circuit is a part of neuronal substrates within interconnected brain regions underscoring auditory fear memory.

INTRODUCTION

Classical fear conditioning is a type of associative learning that is widely used to study the mechanisms underlying learning and memory.¹ Fear conditioning involves an unconditioned stimulus (US), such as an aversive footshock inducing unconditioned responses such as freezing behavior, and a conditioned stimulus (CS), such as an acoustic tone that does not induce aversive responses per se.^{2,3} Although the amygdala is known to play central roles, multiple interconnected brain regions, including the hippocampus, prefrontal cortex, and periaqueductal gray (PAG), collectively referred to as the fear network are involved in fear conditioning.^{2,4–6}

Recent studies have highlighted cerebellar roles in non-motor brain functions, including modulation of social behaviors, reward, and depression-like behaviors.^{7–11} Of note, the cerebellum has been implicated in the modulation of classical fear conditioning.^{12,13} For example, a functional magnetic resonance imaging (fMRI) study using a fear conditioning paradigm in healthy human participants demonstrated that the cerebellum was activated in response to the CS and unexpected US omission after conditioning.¹⁴ Inactivating either the cerebellar cortex or deep cerebellar nuclei (DCNs), which constitute the sole output of the cerebellum, impaired the consolidation of fear

memory in rodents.¹⁵ Recent studies have reported that the cerebellar nucleus neurons projecting to the ventrolateral PAG (vLPAG) are crucial for modulating fear behaviors in rodent.^{16–18} Despite accumulating evidence for cerebellar involvement in fear conditioning, the cerebellar output networks modulating fear conditioning remain largely unknown.

Synaptic plasticity within or between the brain regions in the fear network has been proposed as a neurobiological mechanism of fear learning and memory.^{19–25} It has also been reported that fear conditioning induces synaptic plasticity at multiple microcircuits in the cerebellar cortex, including parallel fiber (PF)-Purkinje cell (PC), molecular layer interneuron (MLI)-PC, and MLI-MLI circuits.^{13,20,26,27} However, whether fear learning induces synaptic changes in cerebellar output pathways has never been investigated.

In the present study, we observed that a population of neurons in the DCN sends monosynaptic glutamatergic projections to the lateral parabrachial nucleus (IPBN), which is a center that relays noxious information to nodes in the fear network comprising the amygdala, PAG, and hypothalamus.^{28–32} Since recent studies have highlighted the role of the IPBN in fear conditioning,^{28,33} we hypothesized that the DCN-IPBN circuit might be critically involved in fear conditioning. Using circuit-specific optogenetic manipulations combined with a classical fear conditioning



paradigm, we demonstrate that the DCN-IPBN pathway is required for auditory, but not contextual, fear conditioning. Moreover, we reveal that auditory fear conditioning potentiates the DCN-IPBN synapses. Our findings provide insight into the circuit mechanisms underlying the cerebellar contribution to classical fear conditioning and deepen our understanding of brain-wide fear memory networks distributed among interconnected brain regions.

RESULTS

DCN neurons send monosynaptic glutamatergic projections to the IPBN

To identify brain regions receiving cerebellar projections that modulate fear learning and memory, we injected adeno-associated virus (AAV) harboring EYFP into the DCN and observed robust EYFP signals in the IPBN (Figure 1A). Given that the IPBN is a center for relaying diverse noxious information to other brain regions and plays a critical role in fear memory processing,^{28–30,33–35} we hypothesized that the cerebellum may modulate fear learning and memory via the DCN-IPBN pathway. We examined the distribution of IPBN-projecting neurons among cerebellar nuclei by injecting retro beads into the IPBN (Figures 1B, 1C, and S1). Of the retrogradely labeled neurons in the DCN, 91.20% of labeled cells were ipsilateral to the IPBN (91.20%) and 8.80% were contralateral (Figure 1C). Neurons in the fastigial, interpositus, and dentate nuclei accounted for 3.29%, 70.16%, and 26.56% of ipsilaterally projecting DCN neurons, respectively (Figure 1C).

To validate the functional connectivity between the DCN and IPBN, we expressed channelrhodopsin-2 (ChR2) selectively in IPBN-projecting DCN neurons by injecting retrograde AAV-harboring Cre recombinase into the IPBN and AAV-expressing Cre-dependent ChR2 into the DCN in mice (Figure 1D). A brief pulse of blue laser (5 ms) elicited an optogenetically evoked excitatory postsynaptic current (oEPSC) at the DCN-IPBN synapse (Figure 1D). 75.51% of recorded DCN neurons showed oEPSCs, which were completely blocked by tetrodotoxin (TTX), a voltage-gated sodium channel blocker (Figures 1E and 1F). The potassium channel blocker 4-aminopyridine (4-AP) recovered the oEPSCs, demonstrating that cerebellar axons made mono-synaptic connections with IPBN neurons (Figures 1E and 1F). Furthermore, the recovered evoked synaptic currents were re-blocked by 2,3-dihydroxy-6-nitro-7-sulfamoyl-benzo[f]quinoxaline (NBQX), which blocks AMPA (α -amino-3-hydroxy-5-methyl-4-isoxazolepropionic acid)-mediated currents, suggesting that DCN-IPBN synapses are glutamatergic (Figures 1E and 1F).

The IPBN is composed of multiple neuronal cell types.³⁴ To characterize the molecular signature of IPBN neurons receiving inputs from the DCN, we labeled DCN-connected IPBN neurons by injecting AAV expressing the anterograde transneuronal tracer wheat germ agglutinin (WGA) fused to Cre in the DCN and the AAV-harboring Cre-dependent EYFP in the IPBN (Figure 1G). Immunostaining with antibodies for previously reported cell type markers in the IPBN revealed that 90.20%, 63.70%, and 9.87% of EYFP-labeled neurons were positive for pituitary adenylate-cyclase-activating polypeptide (PACAP), forkhead

box protein P2 (FOXP2), and calcitonin gene-related peptide (CGRP), respectively (Figure S2B). Next, we tracked EYFP signals of labeled IPBN neuronal axons to identify the downstream target regions of the DCN-IPBN circuit. Identified targets of the DCN-IPBN pathway included the lateral hypothalamus (LH), the paraventricular nucleus of the hypothalamus (PVH), the bed nucleus of the stria terminalis (BNST), the central amygdala (CeA), and the PAG, which are involved in fear memory processing (Figures 1H and S2C). Of note, EYFP signals were not detected in either the lateral or basolateral amygdala (Figure S2C). To examine whether the EYFP signals label direct downstream targets or *en passant* fibers, we labeled DCN-connected IPBN neurons by injecting anterograde AAV1-expressing Cre into the DCN and AAV-expressing Cre-dependent synaptophysin fused to mRuby into the IPBN (Figure 1I). Consistent with the EYFP tracking data, we found that mRuby signals are also detected in the fear-related brain regions (Figure 1J).

DCN \rightarrow IPBN neurons are necessary for auditory fear memory

To examine the involvement of the DCN-IPBN circuit in fear memory processing, we expressed halorhodopsin (NpHR) and optogenetically inhibited DCN \rightarrow IPBN neurons during fear learning and retrieval (Figure 2A). We tested mice using the classical fear conditioning paradigm where mice were trained with auditory tone and footshock pairings (Figures 2B and 2F). The DCN \rightarrow IPBN neurons were optogenetically inactivated during cued and contextual memory retrieval sessions 1 day after fear conditioning (Figures 2B–2E). NpHR-expressing mice exhibited significantly less freezing behavior compared with control EYFP-expressing mice in the cued memory retrieval test with yellow laser delivery (Figure 2D). Both groups exhibited comparable levels of freezing in the contextual fear memory test with yellow laser delivery (Figure 2E), indicating that the DCN-IPBN circuit is required for cued, but not contextual, fear memory retrieval. Next, we optogenetically inactivated DCN \rightarrow IPBN neurons in the training session and examined freezing responses without applying optogenetic inhibition during fear memory retrieval sessions (Figures 2F–2I). Optogenetic inhibition of DCN \rightarrow IPBN neurons did not affect freezing behavior in the training session (Figure 2G). Although the effect was mild, NpHR-expressing mice exhibited significantly less freezing behavior compared with control mice in the cued fear memory test, showing that suppression of DCN \rightarrow IPBN neurons during the training session also affected auditory fear memory (Figure 2H). Of note, both groups showed comparable levels of freezing in the contextual memory test (Figure 2I). Optogenetic inhibition of DCN axon terminals in the IPBN during the cued memory retrieval test also blocked cued fear memory retrieval (Figure S3). In contrast, optogenetic inhibition of DCN \rightarrow IPBN neurons did not affect innate fear responses to fox urine, locomotor activity, anxiety levels measured in an open field, mechanical sensitivity, or social interactions (Figure S4).

Activating DCN \rightarrow IPBN neurons induces freezing after auditory fear conditioning

Given the critical role of the IPBN in modulating behavioral responses to dangerous stimuli,^{28,30,33} we assessed whether direct activation of the DCN-IPBN pathway could elicit specific

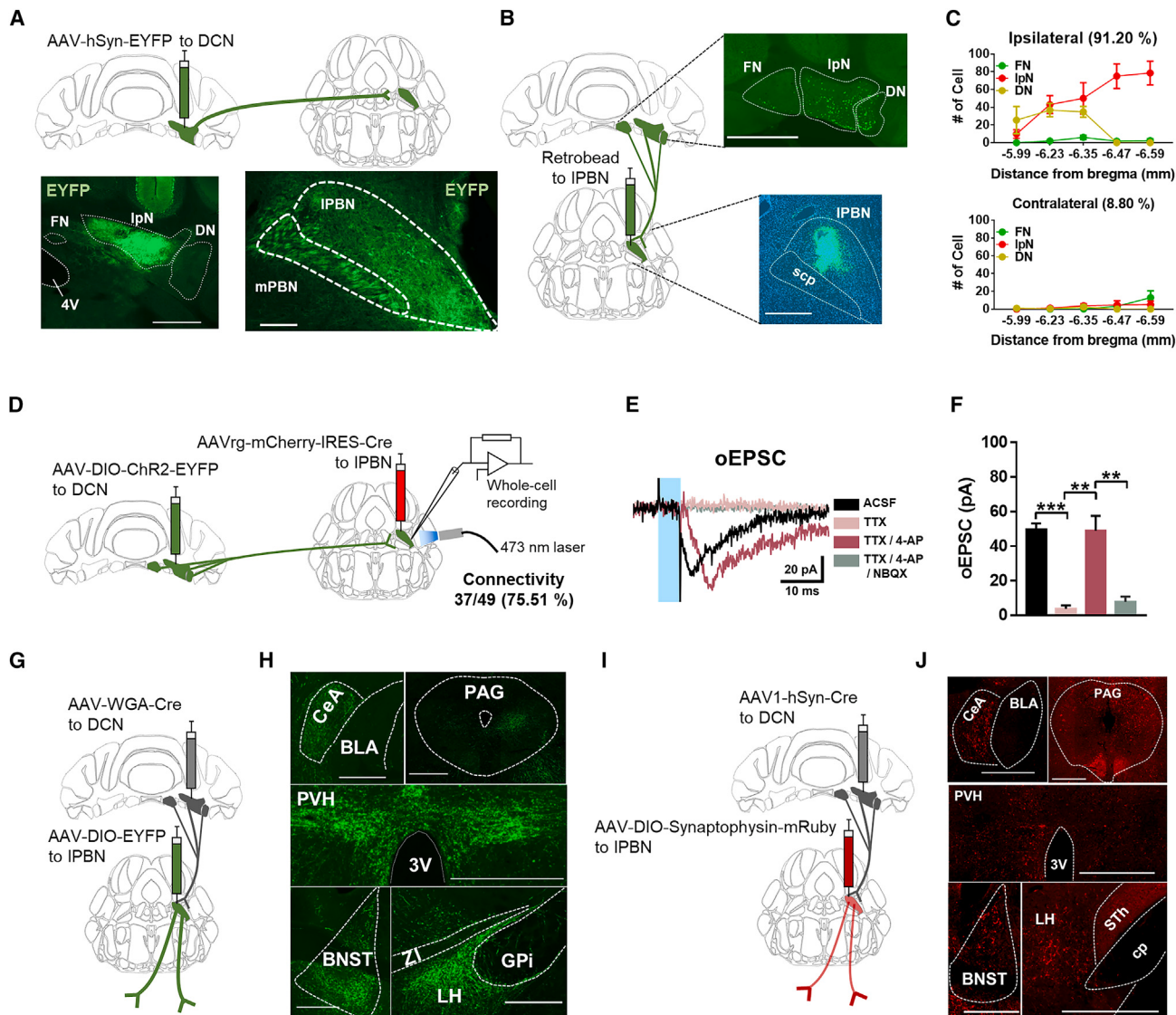


Figure 1. DCN neurons project to the IPBN

- (A) Viral injection of AAV-hSyn-EYFP into the DCN. Left: EYFP expression in the DCN. Right: EYFP signals in the IPBN. Scale bars: 500 μ m (left) and 200 μ m (right).
- (B) Retrograde tracing from the IPBN to DCN. Left: strategy for labeling IPBN-projecting DCN neurons. Right: representative images of retro bead injection into the IPBN and retrogradely labeled DCN neurons. FN, fastigial nucleus; IpN, interpositus nucleus; DN, dentate nucleus. Scale bars: 1 mm (top) and 500 μ m (bottom).
- (C) Number of labeled cells along the rostro-caudal axis ($n = 3$ mice).
- (D) Whole-cell patch-clamp recordings of optogenetically evoked EPSCs (oEPSCs) in the IPBN via stimulation of ChR2-expressing cerebellar axons. Of 49 cells recorded, 37 cells exhibited time-locked synaptic responses to blue laser stimulation.
- (E) Example recording traces of oEPSCs with pharmacological treatment.
- (F) oEPSCs recorded in the IPBN treated with TTX, 4-AP, and NBQX ($n = 5$ slices from 5 mice; ACSF vs. +TTX, two-tailed paired t test, *** $p = 0.0002$; +TTX vs. +4-AP, two-tailed paired t test, ** $p = 0.0036$; +4-AP vs. +NBQX, two-tailed paired t test, ** $p = 0.0088$).
- (G) Anterograde labeling from the DCN to IPBN. AAV8-EF1 α -mCherry-IRES-WGA-Cre and AAV1-EF1 α -DIO-EYFP were injected into the DCN and the IPBN, respectively. The anterograde transneuronal tracer wheat germ agglutinin (WGA) fused to Cre recombinase in the DCN permits EYFP expression in IPBN neurons receiving input from the DCN.
- (H) Representative images of DCN-connected IPBN projections. BLA, basolateral amygdala; BNST, bed nucleus of the stria terminalis; CeA, central amygdala; LH, lateral hypothalamic area; PAG, periaqueductal gray; PVH, paraventricular nucleus of the hypothalamus; GPI, globus pallidus internus; ZI, zona incerta; 3V, third ventricle. Scale bar: 500 μ m.
- (I) Anterograde labeling from the DCN to IPBN using synaptophysin-mRuby. AAV1-hSyn-Cre and AAV1-hSyn-DIO-synaptophysin-mRuby were injected into the DCN and the IPBN, respectively.
- (J) Representative images of synaptophysin-mRuby signals of the DCN-connected IPBN projections. Scale bar: 500 μ m.
- Data are presented as mean \pm SEM.
- See also Figures S1 and S2.

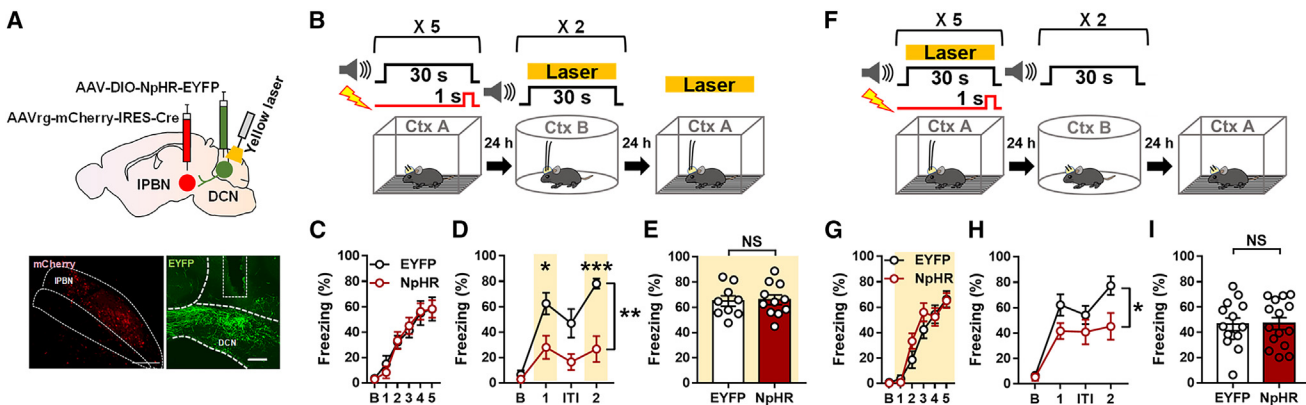


Figure 2. Optogenetic suppression of DCN \rightarrow IPBN neurons impairs auditory fear memory

- (A) Top: Strategy for NpHR expression and optogenetic inhibition in IPBN-projecting DCN neurons. Bottom: representative images of virus expression and optic cannula implantation in the IPBN (left) and the DCN (right). Scale bar: 200 μ m.
- (B) Experimental protocol for fear conditioning and fear memory retrieval paired with optogenetic inhibition.
- (C) Percentage of time spent freezing in response to the conditioned tone during fear conditioning (EYFP, n = 9 mice; NpHR, n = 11 mice; two-way repeated-measures ANOVA, effect of group, $F_{1,18} = 0.0002$, p = 0.9883). B, baseline.
- (D) Percentage of time spent freezing in response to the conditioned tone with optogenetic inhibition during retrieval (EYFP, n = 9 mice; NpHR, n = 11 mice; two-way repeated-measures ANOVA, for group, $F_{1,18} = 15.27$, **p = 0.0010; Bonferroni post-hoc test, tone session 1, *p = 0.0158; tone session 2, ***p = 0.0003). ITI, intertrial interval.
- (E) Percentage of time spent freezing during re-exposure to the training context with constant yellow laser (EYFP, n = 9 mice; NpHR, n = 11 mice; two-tailed unpaired t test, p = 0.8657). NS, not significant.
- (F) Experimental protocols for fear conditioning paired with optogenetic inhibition and fear memory retrieval.
- (G) Percentage of time spent freezing in response to the conditioned tone with optogenetic inhibition during fear conditioning (EYFP, n = 14 mice; NpHR, n = 15 mice; two-way repeated-measures ANOVA, for group, $F_{1,27} = 0.6086$, p = 0.4421).
- (H) Percentage of time spent freezing in response to the conditioned tone during the cued test (EYFP, n = 14 mice; NpHR, n = 15 mice; two-way repeated measures ANOVA, for group, $F_{1,27} = 4.833$, *p = 0.0367; Bonferroni post-hoc test, tone session 1, p = 0.1792; tone session 2, p = 0.0662).
- (I) Percentage of time spent freezing during re-exposure to the training context (EYFP, n = 14 mice; NpHR, n = 15 mice; two-tailed unpaired t test, p = 0.8277). Data are presented as mean \pm SEM.

See also Figures S3 and S4.

behavioral outcomes such as freezing behavior. We expressed ChR2 in DCN \rightarrow IPBN neurons and targeted the DCN for optogenetic stimulation with blue laser delivery (Figure 3A). Mice were placed in a chamber and received three blocks of blue laser stimulation (473 nm, 30 s, 20 Hz) (Figure 3B). Optogenetic stimulation of DCN \rightarrow IPBN neurons did not induce a significant level of freezing in ChR2-expressing mice compared with that in EYFP-expressing mice (Figure 3C). Mice were then re-exposed to the same chamber 24 h after optogenetic stimulation to investigate contextual fear memory formation in ChR2-expressing mice (Figure 3B). However, neither ChR2- nor EYFP-expressing mice exhibited freezing behavior (Figure 3D). Optogenetic stimulation did not induce any changes in locomotor velocity and time spent in the center zone in an open field (Figure S5).

Next, we tested whether activating DCN \rightarrow IPBN neurons after fear conditioning would induce freezing behavior (Figure 3E). Mice were trained by pairing a tone and footshock, followed by optogenetic activation of DCN \rightarrow IPBN neurons the following day (Figures 3F–3I). ChR2-expressing mice exhibited increased freezing behavior in response to optogenetic stimulation compared with control EYFP-expressing mice (Figure 3G). In contrast, both groups demonstrated comparable levels of freezing in response to the tone alone or to concurrent presentation of the tone and laser (Figures 3H and 3I). As optogenetic inhibition of DCN \rightarrow IPBN neurons did not affect contextual fear

memory (Figures 2E and 2I), we assessed whether contextual fear conditioning, in which the tone was not used, would enable optogenetic stimulation-induced freezing after conditioning (Figures 3J–3M). Optogenetic activation of DCN \rightarrow IPBN neurons did not induce freezing behavior after contextual fear conditioning either in ChR2- or EYFP-expressing mice (Figure 3L), and both groups exhibited comparable levels of freezing in the contextual fear memory retrieval test (Figure 3M). Of note, direct activation of IPBN-projecting DCN neurons via intra-DCN injection of ChR2-harboring anterograde transsynaptic AAV1³⁶ induced robust freezing behavior in ChR2-expressing mice (Figure S6).

Potentiation of DCN-IPBN synapses by auditory fear conditioning

Our findings converged into the question of whether auditory fear conditioning strengthens synapses between the DCN and the IPBN. To answer this question, we performed ex vivo whole-cell patch-clamp recordings in mice expressing ChR2 in DCN \rightarrow IPBN neurons. Mice were trained with tone-shock pairings (T + S group) or shock only (S group) or stayed in the home cage (HC group) as a control group (Figure 4A). We recorded oEPSCs in IPBN-containing slices by optically stimulating ChR2-expressing DCN axons in the IPBN 24 h after training (Figure 4A). The oEPSCs recorded in IPBN neurons were significantly increased

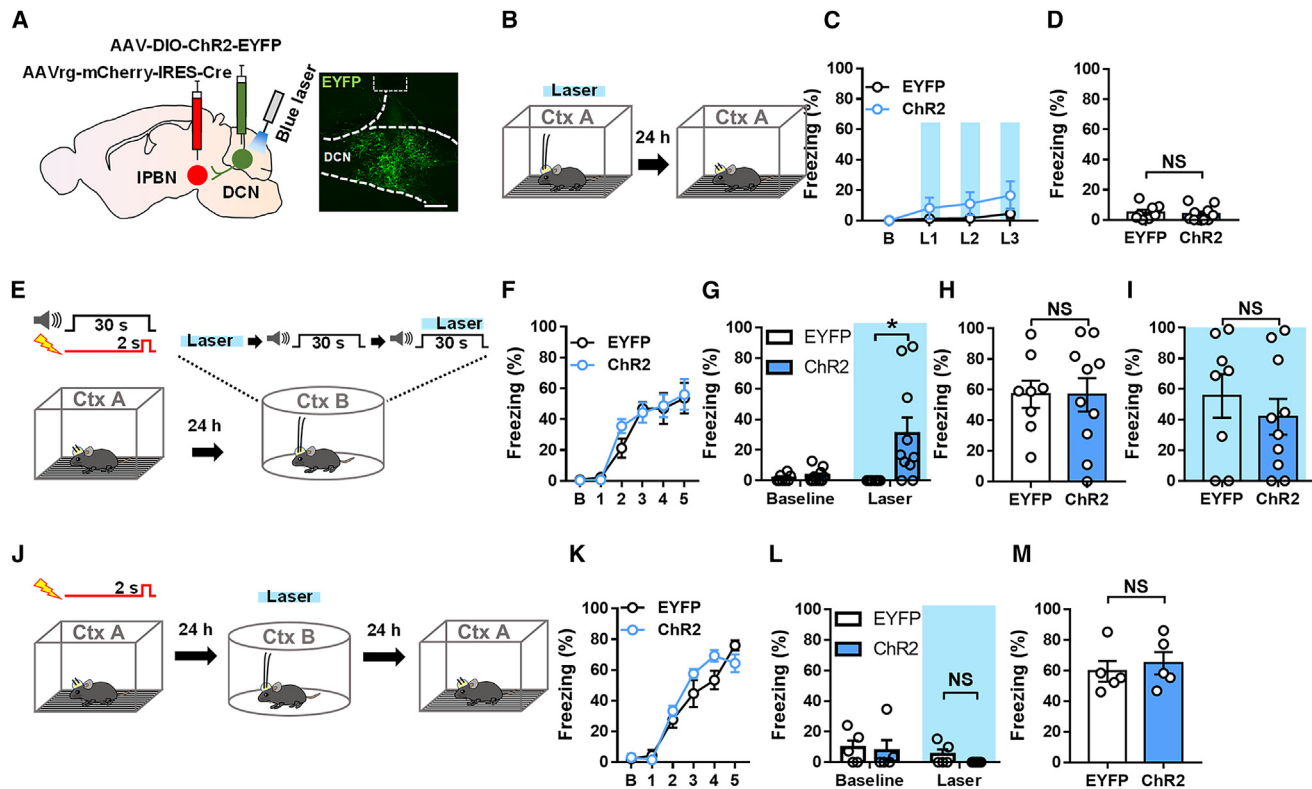


Figure 3. Optogenetic stimulation of DCN \rightarrow IPBN neurons elicits freezing behavior after auditory fear conditioning

- (A) Left: strategy for ChR2 expression and optogenetic activation in IPBN-projecting DCN neurons. Right: representative image of virus expression and optic cannula implantation in the DCN. Scale bar: 200 μ m.
- (B) Experimental protocol for optogenetic activation.
- (C) Time spent freezing in response to three optogenetic stimuli (EYFP, n = 8 mice; ChR2, n = 9 mice; two-way ANOVA, for group, $F_{1,15} = 0.5268$, p = 0.4791). B, baseline; L, laser stimulation.
- (D) Time spent freezing in the same chamber 24 h after optogenetic stimulation (EYFP, n = 8 mice; ChR2, n = 9 mice; two-tailed unpaired t test, p = 0.6964).
- (E) Experimental protocol for optogenetic activation in IPBN-projecting DCN neurons after auditory fear conditioning.
- (F) Percentage of time spent freezing in response to the conditioned tone during fear conditioning (EYFP, n = 8 mice; ChR2, n = 10 mice; two-way repeated-measures ANOVA, effect of group, $F_{1,16} = 0.3091$, p = 0.5859).
- (G) Percentage of time spent freezing before and during optogenetic stimulation (EYFP, n = 8 mice; ChR2, n = 10 mice; two-tailed unpaired t test, *p = 0.0184).
- (H) Percentage of time spent freezing in response to the conditioned tone during the cued memory retrieval test (EYFP, n = 8 mice; ChR2, n = 10 mice; two-tailed unpaired t test, p = 0.9796).
- (I) Percentage of time spent freezing in response to the conditioned tone with optogenetic stimulation (EYFP, n = 8 mice; ChR2, n = 10 mice; two-tailed unpaired t test, p = 0.4676).
- (J) Experimental protocol for optogenetic activation after cue-independent fear conditioning.
- (K) Percentage of time spent freezing during contextual fear conditioning (EYFP, n = 5 mice; ChR2, n = 5 mice; two-way repeated-measures ANOVA, for group, $F_{1,8} = 1.093$, p = 0.3263).
- (L) Percentage of time spent freezing before and during optogenetic stimulation in context B (EYFP, n = 5 mice; ChR2, n = 5 mice; two-tailed unpaired t test, p = 0.1536).
- (M) Percentage of time spent freezing during re-exposure to the training context (EYFP, n = 5 mice; ChR2, n = 5 mice; two-tailed unpaired t test, p = 0.6077).
- Data are presented as mean \pm SEM.

See also Figures S5 and S6.

in the T + S group compared with those in the S and HC groups (Figure 4B). Furthermore, the AMPA/NMDA ratio was significantly higher in the T + S group than that in the S group (Figure S7). Other electrophysiological properties such as input resistance, firing frequency, paired-pulse ratio of oEPSCs, and amplitude and frequency of spontaneous EPSCs (sEPSCs) in IPBN neurons were not significantly different among groups (Figure S8).

To test whether stimulating DCN \rightarrow IPBN neurons would activate more neurons in the IPBN after auditory fear conditioning, we examined c-Fos expression in the IPBN. Mice expressing ChR2 in DCN \rightarrow IPBN neurons were trained with tone-shock pairings (T + S group) or were left in the home cage (HC group) as controls (Figure 4C). The mice were placed in an open field arena 24 h later and received optogenetic stimulation for 1 min to stimulate DCN \rightarrow IPBN neurons, followed by brain dissection for c-Fos

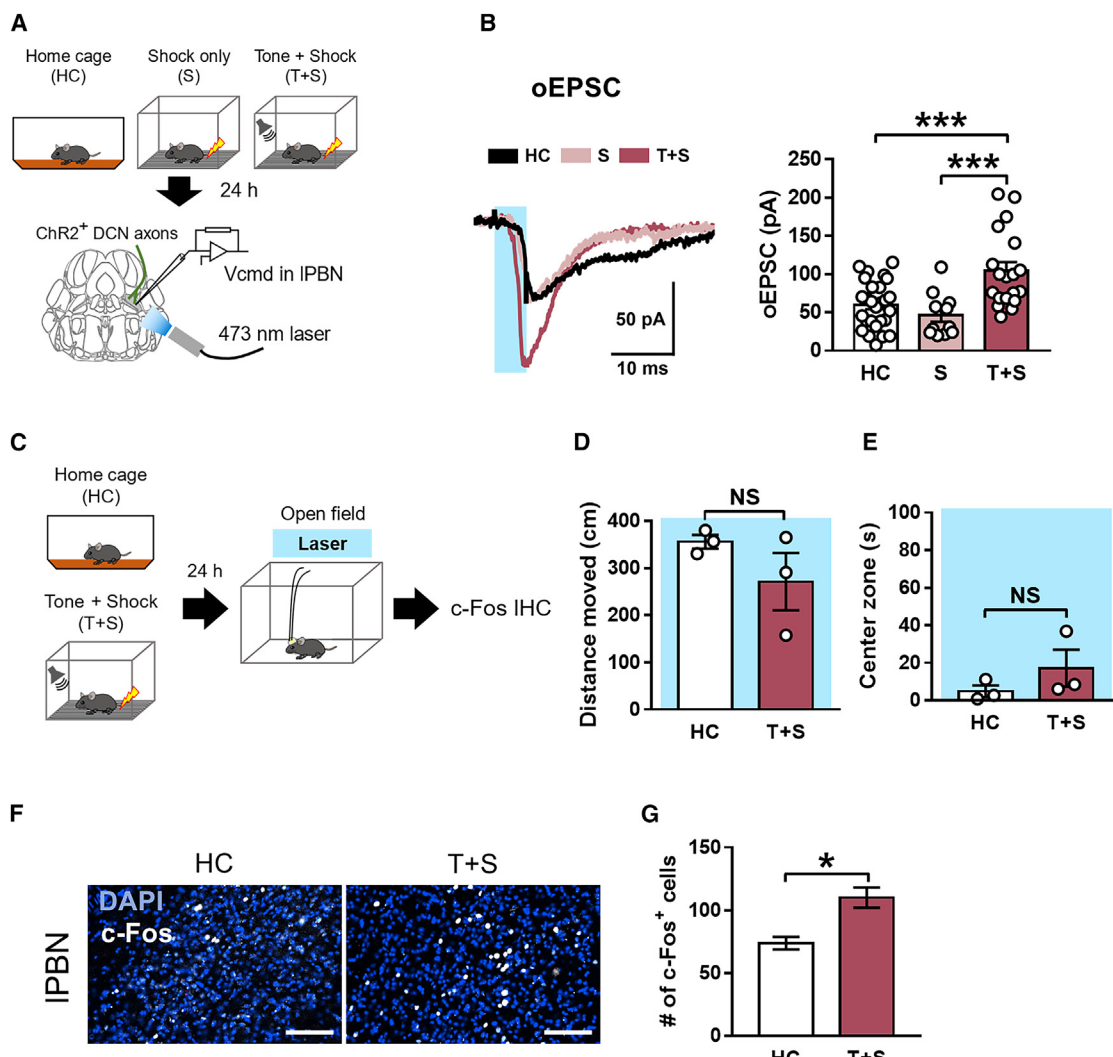


Figure 4. Auditory fear conditioning potentiates the DCN-IPBN pathway

(A) Experimental protocol for *ex vivo* recording in DCN-connected IPBN neurons 24 h after fear conditioning.
(B) Increased synaptic strength in the DCN-IPBN pathway after cued fear learning. Left: example recording traces of oEPSCs. Right: group data for oEPSC recordings in IPBN neurons receiving inputs from the DCN (home cage, n = 27 cells from 5 mice; shock only, n = 11 cells from 3 mice; tone + shock, n = 19 cells from 4 mice; one-way ANOVA, for group, $F_{2, 54} = 11.05$, ***p < 0.0001; Tukey post-hoc test, home cage vs. tone + shock, ***p = 0.0006; shock only vs. tone + shock, ***p = 0.0004; home cage vs. shock only, p = 0.5701).

(C) Behavioral schedules for c-Fos immunohistochemistry after optogenetic stimulation with or without auditory fear conditioning.
(D) Total distance moved in an open field arena with optogenetic stimulation (EYFP, n = 3 mice; NpHR, n = 3 mice; two-tailed unpaired t test, p = 0.2460).
(E) Time spent in the center zone of an open field arena with optogenetic stimulation (EYFP, n = 3 mice; NpHR, n = 3 mice; two-tailed unpaired t test, p = 0.3033).

(F) Representative images of c-Fos expression in the IPBN. Scale bar: 200 μ m.
(G) Summary of c-Fos expression in the IPBN induced by optogenetic stimulation of DCN \rightarrow IPBN neurons in mice that stayed in home cage or conditioned with tone and shock.

Data are presented as mean \pm SEM.

See also Figures S7 and S8.

immunohistochemistry after 90 min (Figure 4C). c-Fos expression in the IPBN was significantly increased in the T + S group compared with that in the HC group, indicating that auditory fear conditioning enhanced synaptic efficacy at the DCN-IPBN pathway, thereby permitting DCN stimulation to activate more neurons in the IPBN (Figures 4F and 4G).

DCN-connected IPBN neurons exhibit conditioned responses to auditory tone

To monitor neural activity in IPBN neurons receiving input from the DCN during fear learning and retrieval sessions, we performed *in vivo* fiber photometry calcium imaging. We expressed the genetically encoded calcium indicator

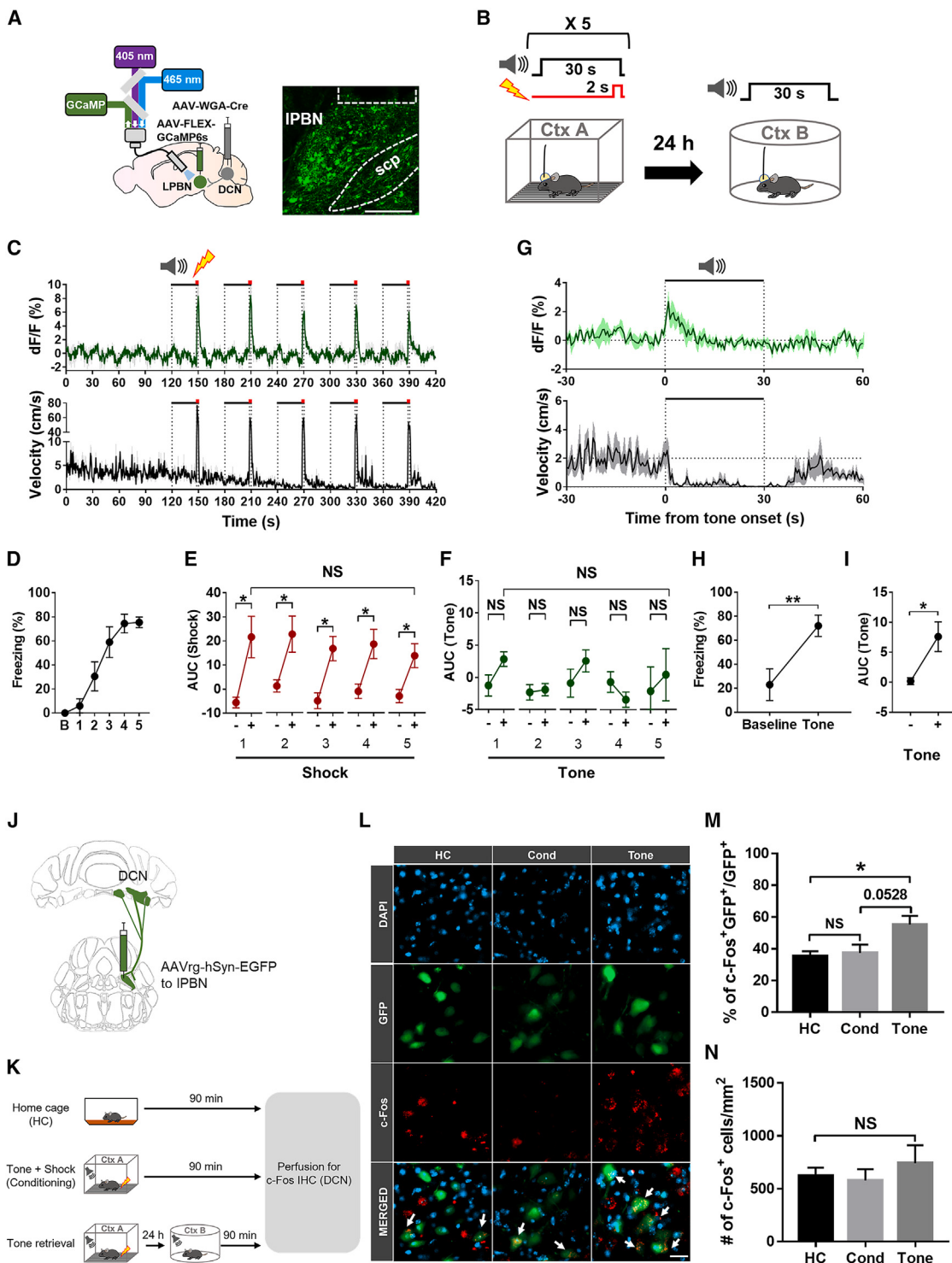


Figure 5. Activity of the DCN-IPBN pathway during fear learning and retrieval

(A) Left: experimental setup and strategy for fiber photometry recordings in DCN-connected IPBN neurons. Right: representative image following virus expression and optic cannula implantation in the IPBN. Scale bar: 200 μ m.

(B) Experimental protocol for auditory fear conditioning.

(C) Average GCaMP6s signal in DCN-connected IPBN neurons (top) and velocity of mice (bottom) during auditory fear conditioning. Black line indicates the time window (30 s) for an auditory stimulus. Red line indicates the time window (2 s) for a footshock stimulus.

(D) Freezing curve during auditory fear conditioning (n = 6 mice).

(legend continued on next page)

GCaMP6s in DCN-connected IPBN neurons and recorded Ca²⁺ signals in the IPBN (Figure 5A). Mice were trained with five tone-shock pairings in a training session, and auditory fear memory was tested in a novel context 24 h after training (Figure 5B). During training, DCN-connected IPBN neurons exhibited robust Ca²⁺ activity in response to footshocks but did not show any significant response to the tone, whereas mice exhibited increased freezing to tone presentations (Figures 5C–5F). Notably, the DCN-connected IPBN neurons exhibited significantly increased Ca²⁺ signals in response to the conditioned tone compared with that before tone presentation during retrieval session (Figures 5G–5I), which is consistent with the *ex vivo* data demonstrating auditory fear learning-induced potentiation of the DCN-IPBN pathway (Figure 4). These results indicate that the DCN-connected IPBN neurons acquired a conditioned response (CR) to the auditory tone after fear conditioning. Of note, the DCN-connected IPBN neurons did not show increased Ca²⁺ signals in response to the unpaired tone, excluding the possibility of non-selective activation of these neurons after fear conditioning (Figure S9).

To investigate whether the DCN^{→IPBN} neurons are also activated during fear conditioning, we performed c-Fos immunohistochemistry in the brain slices containing the DCN after auditory fear conditioning or tone memory retrieval (Figures 5K and 5L). The DCN^{→IPBN} neurons were labeled by injecting a retrograde AAV-expressing EGFP into the IPBN, and mice left in the home cage were used as controls (Figures 5J and 5K). We found that the probability of detecting c-Fos in the DCN^{→IPBN} neurons was significantly higher in the tone memory retrieval group than the HC group (Figure 5M), indicating that DCN^{→IPBN} neurons became more responsive to the conditioned tone after auditory fear conditioning. Interestingly, the overall c-Fos expression was not significantly different among groups (Figure 5N).

Optogenetic stimulation of DCN^{→IPBN} neurons paired with footshock induces conditioned freezing

Our behavioral and electrophysiological data suggested that the DCN-IPBN pathway was critically involved in auditory fear learning and memory but not contextual fear conditioning. It is known that multiple types of sensory information including auditory stimuli are conveyed to and processed in the cerebellum.³⁷ We thus hypothesized that the DCN-IPBN pathway may contribute to the processing of conditioned auditory stimuli and that activating DCN^{→IPBN} neurons could replace the auditory tone in auditory fear conditioning. To test this hypothesis, we optogenetically stimulated ChR2-expressing DCN^{→IPBN} neurons in place of the auditory tone in the classical fear conditioning paradigm (Figures 6A and 6B). Mice expressing ChR2 in DCN^{→IPBN} neurons were trained with either optogenetic stimulation of DCN^{→IPBN} neurons paired with electrical shocks (L + S group) or footshock only (S group). Both groups exhibited comparable levels of freezing after footshocks during training (Figure 6C). Compared with the S group, the L + S group exhibited significantly more freezing behavior upon optogenetic stimulation in a novel context 24 h after training (Figure 6D). Both groups demonstrated comparable levels of freezing in the contextual fear memory test, indicating that both groups learned well (Figure 6E). In a control experiment, optogenetic stimulation of DCN^{→IPBN} neurons did not affect freezing behavior during either training or retrieval in EYFP-expressing mice, ruling out the possibility that light functions as a visible CS associated with footshock (Figures 6F–6H). Furthermore, when mice expressing ChR2 in DCN^{→IPBN} neurons were trained with optogenetic stimulation of DCN^{→IPBN} neurons paired with auditory tone, the mice did not show freezing behaviors in response to the tone 24 h after training (Figure S10). Collectively, these data indicated that the auditory tone (CS) but not footshock (US) could be replaced with activation of DCN^{→IPBN} neurons in the auditory fear conditioning paradigm.

(E) Area under the curve (AUC) of calcium activity in DCN-connected IPBN neurons during footshocks compared with that before shock delivery in the auditory fear training session. Calcium activity during 5 s before (–) and after (+) footshock was analyzed ($n = 6$ trials in 6 mice; two-tailed paired t test, session 1, * $p = 0.0389$; session 2, * $p = 0.0220$; session 3, * $p = 0.0185$; session 4, * $p = 0.0318$; session 5, * $p = 0.0371$; one-way repeated-measures ANOVA, for group, $F_{1,228} = 6.139$, $p = 0.1444$).

(F) AUC of calcium activity in DCN-connected IPBN neurons during tone presentation compared with that before tone presentation in the auditory fear training session. Calcium activity during 5 s before (–) and after (+) tone presentation was analyzed ($n = 6$ trials in 6 mice; two-tailed paired t test, session 1, $p = 0.0508$; session 2, $p = 0.5847$; session 3, $p = 0.1184$; session 4, $p = 0.2405$; session 5, $p = 0.2563$; one-way repeated-measures ANOVA, for group, $F_{1,532,7661} = 1.633$, $p = 0.2516$).

(G) Average GCaMP6s signals in DCN-connected IPBN neurons (top) and velocity of mice (bottom) during auditory fear memory retrieval. Black line indicates the time window (30 s) for an auditory stimulus.

(H) Freezing during the baseline period and tone presentation in the auditory fear memory retrieval session with fiber photometry calcium imaging ($n = 6$ mice; two-tailed paired t test, ** $p = 0.0037$).

(I) AUC of calcium activity in DCN-connected IPBN neurons during tone presentation compared with that before tone presentation in the auditory fear memory retrieval test. Calcium activity during 5 s before (–) and after (+) tone presentation was analyzed ($n = 6$ trials in 6 mice per session; two-tailed paired t test, * $p = 0.0342$).

(J) Strategy for retrograde labeling of IPBN-projecting DCN neurons.

(K) Experimental protocol for c-Fos immunohistochemistry.

(L) Representative images of EGFP-expressing IPBN-projecting DCN neurons immunostained with c-Fos. HC, home cage control; Cond, auditory fear conditioning; Tone, auditory tone retrieval. Scale bar: 20 μ m.

(M) Proportion of c-Fos⁺ IPBN-projecting DCN neurons (HC, $n = 5$ mice; Cond, $n = 4$ mice; Tone, $n = 5$ mice; one-way ANOVA, for group, $F_{2,11} = 5.797$, * $p = 0.0191$; Tukey post-hoc test, HC vs. Cond, $p = 0.9594$; HC vs. Tone, * $p = 0.0243$; Cond vs. Tone, $p = 0.0528$).

(N) Total count of c-Fos⁺ cells in each group (HC, $n = 5$ mice; Cond, $n = 4$ mice; Tone, $n = 5$ mice; one-way ANOVA, for group, $F_{2,11} = 0.4380$, $p = 0.6561$). Data are presented as mean \pm SEM.

See also Figure S9.

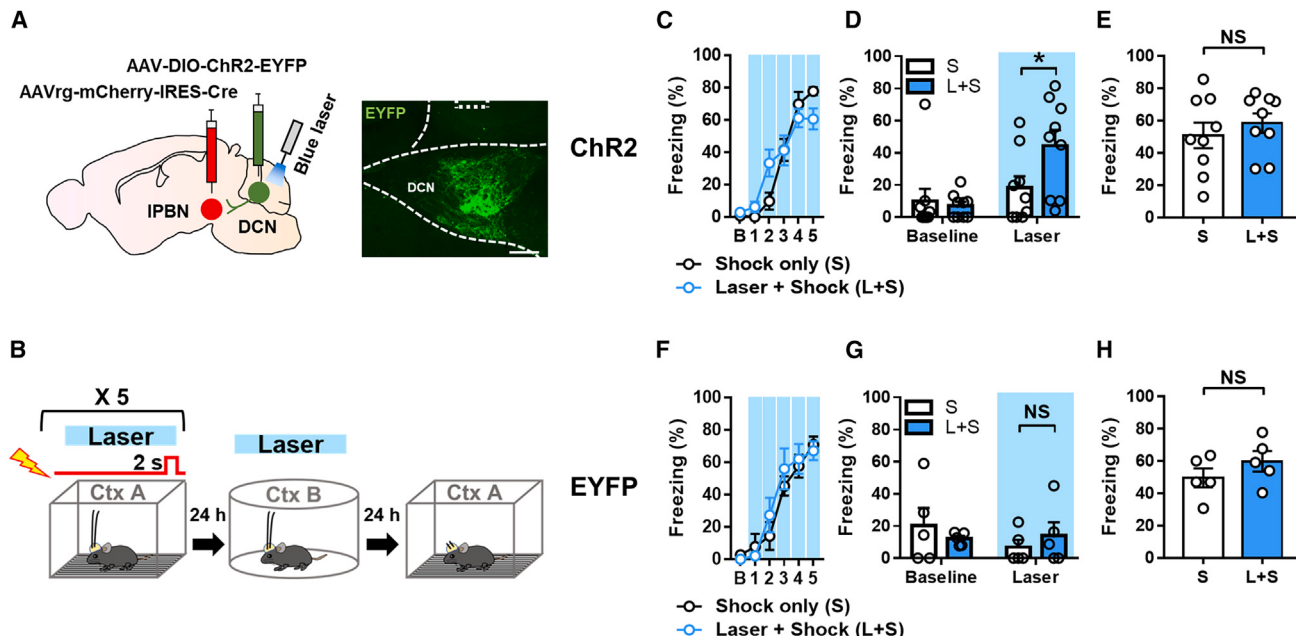


Figure 6. Optogenetic stimulation of DCN \rightarrow IPBN neurons paired with footshock induces conditioned freezing

- (A) Left: strategy for ChR2 expression and optogenetic activation in IPBN-projecting DCN neurons. Right: representative image of virus expression and optic cannula implantation in the DCN. Scale bar: 200 μ m.
- (B) Experimental protocol for optogenetic stimulation paired with footshocks for fear conditioning.
- (C) Percentage of time spent freezing in response to optogenetic stimulation during fear conditioning in ChR2-expressing mice (shock only [S], n = 9 mice; laser + shock [L + S], n = 9 mice; two-way repeated-measures ANOVA, for group, $F_{1,16} = 0.0180$, p = 0.8948).
- (D) Percentage of time spent freezing before and during optogenetic stimulation after fear conditioning in ChR2-expressing mice (S, n = 9 mice; L + S, n = 9 mice; two-tailed unpaired t test, *p = 0.0482).
- (E) Percentage of time spent freezing during re-exposure to the training context in ChR2-expressing mice (S, n = 9 mice; L + S, n = 9 mice; two-tailed unpaired t test, p = 0.4590).
- (F) Percentage of time spent freezing in response to optogenetic stimulation during fear conditioning in EYFP-expressing mice (S, n = 5 mice; L + S, n = 5 mice; two-way repeated-measures ANOVA, for group, $F_{1,8} = 0.1985$, p = 0.6678).
- (G) Percentage of time spent freezing before and during optogenetic stimulation after fear conditioning in EYFP-expressing mice (S, n = 5 mice; L + S, n = 5 mice; two-tailed unpaired t test, p = 0.4663).
- (H) Percentage of time spent freezing during re-exposure to the training context in EYFP-expressing mice (S, n = 5 mice; L + S, n = 5 mice; two-tailed unpaired t test, p = 0.2709).

Data are presented as mean \pm SEM.

See also Figure S10.

DISCUSSION

The classical fear conditioning paradigm is widely used to study the neurobiological mechanisms underlying fear learning and memory from molecular to systems levels.⁵ Most studies on fear memory have focused on forebrain regions functionally interconnected with the amygdala.^{2,38} However, accumulating evidence indicates that fear memories are processed and stored in distributed networks in the entire brain, including the cerebellum and brainstem nuclei.^{12,14,28,39,40} Our study revealed that the cerebellum modulates classical fear conditioning via its projections to the IPBN. The IPBN is a brain region critical for generating appropriate defensive behaviors in response to noxious stimuli.^{28–30} IPBN neurons, particularly CGRP-expressing (CGRP $^+$) neurons, are robustly activated by nociception, food neophobia, and threat and relay this noxious information to connected brain areas, such as the hypothalamus, the CeA, the thalamus, and the PAG, to orchestrate nocifensive be-

haviors.^{30,33,41} Of note, although CGRP $^+$ neurons in the IPBN become responsive to a CS once it is associated with an aversive US, how sensory signals associated with the US are conveyed to the IPBN is not known.^{33,34} Here, we observed that IPBN neurons receiving input from the DCN exhibited GCaMP signals to an auditory tone associated with an electric footshock, indicating that the cerebellum conveys CS information to the IPBN to elicit CRs such as freezing by activating the connected areas such as the CeA. Consistently, we found that optogenetic activation of DCN \rightarrow IPBN neurons can replace auditory tone, but not footshock, in auditory fear conditioning.

We observed that PACAP $^+$ neurons in the IPBN, rather than CGRP $^+$ neurons, predominantly received cerebellar projections. PACAP $^+$ neurons have been implicated in anxiety-like behaviors and posttraumatic stress disorder (PTSD).^{42,43} Our tracing results revealed that IPBN neurons receiving inputs from the DCN projected to multiple brain regions implicated in the modulation of fear, anxiety, and freezing behaviors, including the CeA

and the PAG. Collectively, the anatomical and functional data presented herein, in conjunction with previous findings in humans and animals,^{12–14} strongly suggest that the DCN-IPBN pathway is a component of distributed fear memory networks.

We found that optogenetic inhibition of the DCN-IPBN pathway selectively impaired auditory fear memory without affecting contextual fear memory. This is consistent with previous reports demonstrating that the cerebellum is critical for modulating auditory fear memory. For example, inactivating the interpositus nucleus impairs the consolidation of auditory fear memory without affecting contextual fear memory.¹⁵ *Hot-foot* mice, which have deficits in PF-PC synapses, exhibit a selective deficit in auditory fear memory.²⁰ Furthermore, a recent study using PC-specific STAT3 knockout mice reported that cerebellum-specific genetic manipulation affects auditory fear memory without affecting contextual fear memory.⁴⁴ The cerebellum is critical for encoding sensory prediction error and timing, thereby contributing to associative learning paradigms such as reward learning and eyeblink conditioning. As such, the cerebellum likely enables animals to make appropriate responses to sensory cues associated with aversive stimuli.^{45,46} Our other findings also support the notion that the DCN-IPBN pathway is selectively involved in processing auditory fear memory. First, activating DCN \rightarrow IPBN neurons induced freezing behaviors after auditory fear conditioning but not after contextual fear conditioning. Second, auditory fear conditioning, but not contextual fear conditioning, potentiated DCN-IPBN synapses. While previous studies have suggested that the cerebellum interacts with the hippocampus and modulates hippocampus-dependent cognitive functions including contextual fear memory,^{47–50} we found that acute manipulation of DCN-IPBN activity did not affect hippocampal function. Since our study predominantly targeted the interpositus nucleus, the modulatory roles of cerebellar nuclei projecting to other brain regions in contextual fear conditioning warrant further investigation.

Activation of DCN \rightarrow IPBN neurons induced freezing behaviors only after auditory fear conditioning, suggesting that auditory fear conditioning modulates DCN-IPBN synapses. Indeed, our *ex vivo* electrophysiology, c-Fos immunohistochemistry, and *in vivo* fiber photometry calcium imaging data provide converging evidence demonstrating that auditory fear conditioning potentiates the DCN-IPBN synapses. Similarly, fear conditioning-induced synaptic plasticity has been demonstrated in other brain regions including the amygdala, hippocampus, and cerebellar cortex, highlighting these synaptic changes as a potential cellular mechanism of fear memory.^{19–22} Particularly, the lateral amygdala (LA) has been suggested as a core site where the plasticity underlying auditory fear conditioning occurs.^{23–25} However, CS-US association and plasticity also occur in brain regions other than the LA during fear conditioning. For example, a recent study showed that calretinin-expressing neurons in the auditory thalamus integrate CS-US representations and provide them to the LA.⁵¹ CGRP receptor-expressing neurons in the lateral division of the CeA are also suggested as a site of convergence of CS and US.²⁸ Our results suggest that the DCN neurons play a role in conveying the association of CS and US signals to the IPBN, contributing to the expansion of the concept of a distributed fear memory network.

According to a classical view of fear conditioning, the CS (auditory tone) is reported to be relayed from the cochlea to the auditory thalamus and auditory cortex via the inferior colliculus (IC) and then transmitted to the LA.^{4,52,53} It is known that the cerebellum receives auditory inputs mainly through mossy fibers from the pontine nuclei, which receive neural inputs from the IC, the medial geniculate body, and the auditory cortex.^{54,55} Consistently, previous studies using an eyeblink conditioning paradigm have demonstrated that an auditory tone and aversive CS such as air puff to the eyes are conveyed to the DCN from the pontine nuclei and inferior olive (IO), respectively.^{56,57} However, whether the same upstream neural circuits are engaged in the classical fear conditioning paradigm remains unclear.

Recent studies have reported that cerebellar projections to the vIPAG modulate freezing behavior and fear learning and memory.^{16–18} Several differences exist between the DCN-IPBN and DCN-vIPAG pathways. First, anatomically, the IPBN neurons studied herein receive afferents predominantly from interpositus nucleus neurons, whereas the vIPAG receives inputs from fastigial nuclei neurons in the DCN.^{16–18} Second, our data indicate that the DCN-IPBN pathway regulates auditory fear memory retrieval, whereas the DCN-vIPAG pathway regulates auditory fear memory extinction.^{16,17} Third, regarding the direction of freezing behavior regulation, our data suggest that the DCN-IPBN pathway positively regulates freezing, whereas the DCN-vIPAG pathway negatively regulates freezing.¹⁸ Neurons in the vIPAG project to Purkinje neurons in lobule VIII of the cerebellar vermis through the IO.⁵⁸ This vIPAG-IO-lobule VIII circuit has been reported to regulate muscle tone for fear-evoked freezing behavior.⁵⁸ Moreover, inactivating the cerebellar vermis, which is the main input to the fastigial nucleus, abolished both innate and conditioned freezing behaviors.⁵⁸ Of note, inhibiting the DCN-IPBN pathway did not affect locomotion, anxiety-like behavior assessed in an open field arena, or freezing responses to fox urine. Further, activating DCN \rightarrow IPBN neurons in mice did not induce freezing behaviors per se or alter time spent in the center zone of an open field, indicating that this pathway does not simply modulate motor behaviors including freezing or affect anxiety-like behaviors in mice. Given that three cerebellar nuclei have distinct projection and gene expression patterns, it is plausible that the cerebellar nuclei play distinct modulatory roles in specific aspects or phases of fear conditioning.^{13,59}

Collectively, we identified a cerebellar output pathway involved in classical fear conditioning and provide physiological insights into the role of the cerebellum in fear conditioning. Given that cerebellar dysfunction is associated with multiple non-motor brain disorders such as autism spectrum disorder and PTSD,^{10,60} our study sheds light on the functional organization of brain-wide fear memory networks as well as the pathophysiology of cerebellum-associated affective disorders.

Limitation of the study

While our study strongly suggests that the DCN conveys auditory CS information to the IPBN, we were not able to directly record the activity of the IPBN-projecting DCN neurons to show that the auditory CS is delivered to these neurons during fear conditioning. Also, the specific afferent inputs providing CS and US information to the DCN during fear conditioning are not clear.

Whether the CS and US pathways in eyeblink conditioning are also engaged in the classical fear conditioning paradigm needs to be investigated. Moreover, considering that multiple sensory modalities are conveyed and processed in the cerebellum,^{45,56,61,62} we cannot exclude the possibility that the DCN-IPBN pathway is also responsive to other sensory modalities, such as visual stimulation, in addition to auditory tones. Lastly, a recent study showed that animals can acquire CRs to optogenetic stimuli regardless of the perturbed brain area.⁶³ Although our results showing bidirectional manipulations of the DCN neuronal activity have the opposite effects on fear memory argue that the effects of our optogenetic manipulations are circuit specific, we cannot completely exclude the possibility of “optoception” in our experiments.

STAR★METHODS

Detailed methods are provided in the online version of this paper and include the following:

- **KEY RESOURCES TABLE**

- **RESOURCE AVAILABILITY**

- Lead contact
- Materials availability
- Data and code availability

- **EXPERIMENTAL MODEL AND SUBJECT DETAILS**

- Animals
- **METHOD DETAILS**

 - Stereotaxic surgeries
 - Fear conditioning and optogenetic manipulation
 - Fox urine exposure
 - Von frey test
 - Social interaction
 - Open field test
 - Fiber photometry
 - Electrophysiology
 - Tissue fixation and sectioning
 - Histology

- **QUANTIFICATION AND STATISTICAL ANALYSIS**

SUPPLEMENTAL INFORMATION

Supplemental information can be found online at <https://doi.org/10.1016/j.celrep.2023.112291>.

ACKNOWLEDGMENTS

The authors thank Dr. J.-H. Han and J. Han for helping to establish the fiber photometry system and Dr. S.-B. Paik and W. Choi for supporting imaging analysis. The authors also thank Dr. J.-S. Choi and Dr. J.W. Koo for constructive discussions. This work was supported by grants from the National Research Foundation of Korea (NRF-2022M3E5E8018049, NRF-2019R1A2C1084232, and NRF-2018R1A5A2025964) and by the KBRI basic research program through the Korea Brain Research Institute funded by Ministry of Science and ICT (23-BR-04-03).

AUTHOR CONTRIBUTIONS

Project design, K.-D.H., S.J.K., and Y.-S.L.; supervision, Y.-S.L. and S.J.K.; surgery, K.-D.H.; behavioral experiments with optogenetics and fiber photometry recording, K.-D.H., J.B., J.L., and S.Y.K.; electrophysiological experi-

ments, K.-D.H. and H.G.S.; immunohistochemistry experiments, K.-D.H., J.B., and H.-H.R.; manuscript writing, K.-D.H., S.J.K., and Y.-S.L.; data analysis and interpretation, K.-D.H., J.B., S.J.K., and Y.-S.L.

DECLARATION OF INTERESTS

The authors declare no competing interests.

Received: July 21, 2022

Revised: February 4, 2023

Accepted: March 6, 2023

Published: March 22, 2023

REFERENCES

1. Schafe, G.E., Nader, K., Blair, H.T., and LeDoux, J.E. (2001). Memory consolidation of Pavlovian fear conditioning: a cellular and molecular perspective. *Trends Neurosci.* 24, 540–546. [https://doi.org/10.1016/s0166-2236\(00\)01969-x](https://doi.org/10.1016/s0166-2236(00)01969-x).
2. Tozote, P., Fadok, J.P., and Lüthi, A. (2015). Neuronal circuits for fear and anxiety. *Nat. Rev. Neurosci.* 16, 317–331. <https://doi.org/10.1038/nrn3945>.
3. Myers, K.M., and Davis, M. (2007). Mechanisms of fear extinction. *Mol. Psychiatry* 12, 120–150. <https://doi.org/10.1038/sj.mp.4001939>.
4. LeDoux, J.E. (2000). Emotion circuits in the brain. *Annu. Rev. Neurosci.* 23, 155–184. <https://doi.org/10.1146/annurev.neuro.23.1.155>.
5. Maren, S. (2001). Neurobiology of Pavlovian fear conditioning. *Annu. Rev. Neurosci.* 24, 897–931. <https://doi.org/10.1146/annurev.neuro.24.1.897>.
6. Medina, J.F., Repa, J.C., Mauk, M.D., and LeDoux, J.E. (2002). Parallels between cerebellum- and amygdala-dependent conditioning. *Nat. Rev. Neurosci.* 3, 122–131. <https://doi.org/10.1038/nrn728>.
7. Kang, S., Jun, S., Baek, S.J., Park, H., Yamamoto, Y., and Tanaka-Yamamoto, K. (2021). Recent advances in the understanding of specific efferent pathways emerging from the cerebellum. *Front. Neuroanat.* 15, 759948. <https://doi.org/10.3389/fnana.2021.759948>.
8. Baek, S.J., Park, J.S., Kim, J., Yamamoto, Y., and Tanaka-Yamamoto, K. (2022). VTA-projecting cerebellar neurons mediate stress-dependent depression-like behaviors. *eLife* 11, e72981. <https://doi.org/10.7554/eLife.72981>.
9. Carta, I., Chen, C.H., Schott, A.L., Dorizan, S., and Khodakham, K. (2019). Cerebellar modulation of the reward circuitry and social behavior. *Science* 363, eaav0581. <https://doi.org/10.1126/science.aav0581>.
10. Kelly, E., Meng, F., Fujita, H., Morgado, F., Kazemi, Y., Rice, L.C., Ren, C., Escamilla, C.O., Gibson, J.M., Sajadi, S., et al. (2020). Regulation of autism-relevant behaviors by cerebellar-prefrontal cortical circuits. *Nat. Neurosci.* 23, 1102–1110. <https://doi.org/10.1038/s41593-020-0665-z>.
11. Wagner, M.J., and Luo, L. (2020). Neocortex-cerebellum circuits for cognitive processing. *Trends Neurosci.* 43, 42–54. <https://doi.org/10.1016/j.tins.2019.11.002>.
12. Apps, R., and Strata, P. (2015). Neuronal circuits for fear and anxiety — the missing link. *Nat. Rev. Neurosci.* 16, 642. <https://doi.org/10.1038/nrn4028>.
13. Hwang, K.-D., Kim, S.J., and Lee, Y.-S. (2022). Cerebellar circuits for classical fear conditioning. *Front. Cell. Neurosci.* 16, 836948. <https://doi.org/10.3389/fncel.2022.836948>.
14. Ernst, T.M., Brol, A.E., Gratz, M., Ritter, C., Bingel, U., Schlammann, M., Manderwald, S., Quick, H.H., Merz, C.J., and Timmann, D. (2019). The cerebellum is involved in processing of predictions and prediction errors in a fear conditioning paradigm. *eLife* 8, e46831. <https://doi.org/10.7554/eLife.46831>.
15. Sacchetti, B., Baldi, E., Lorenzini, C.A., and Bucherelli, C. (2002). Cerebellar role in fear-conditioning consolidation. *Proc. Natl. Acad. Sci. USA* 99, 8406–8411. <https://doi.org/10.1073/pnas.112660399>.
16. Frontera, J.L., Baba Aissa, H., Sala, R.W., Mailhes-Hamon, C., Georgescu, I.A., Léna, C., and Popa, D. (2020). Bidirectional control of fear memories by

- cerebellar neurons projecting to the ventrolateral periaqueductal grey. *Nat. Commun.* 11, 5207. <https://doi.org/10.1038/s41467-020-18953-0>.
17. Lawrenson, C., Paci, E., Pickford, J., Drake, R.A.R., Lumb, B.M., and Apps, R. (2022). Cerebellar modulation of memory encoding in the periaqueductal grey and fear behaviour. *eLife* 11, e76278. <https://doi.org/10.7554/eLife.76278>.
 18. Vaaga, C.E., Brown, S.T., and Raman, I.M. (2020). Cerebellar modulation of synaptic input to freezing-related neurons in the periaqueductal gray. *eLife* 9, e54302. <https://doi.org/10.7554/eLife.54302>.
 19. McKernan, M.G., and Shinnick-Gallagher, P. (1997). Fear conditioning induces a lasting potentiation of synaptic currents in vitro. *Nature* 390, 607–611. <https://doi.org/10.1038/37605>.
 20. Sacchetti, B., Scelfo, B., Tempia, F., and Strata, P. (2004). Long-Term synaptic changes induced in the cerebellar cortex by fear conditioning. *Neuron* 42, 973–982. <https://doi.org/10.1016/j.neuron.2004.05.012>.
 21. Nabavi, S., Fox, R., Proulx, C.D., Lin, J.Y., Tsien, R.Y., and Malinow, R. (2014). Engineering a memory with LTD and LTP. *Nature* 511, 348–352. <https://doi.org/10.1038/nature13294>.
 22. Johansen, J.P., Cain, C.K., Ostroff, L.E., and LeDoux, J.E. (2011). Molecular mechanisms of fear learning and memory. *Cell* 147, 509–524. <https://doi.org/10.1016/j.cell.2011.10.009>.
 23. Quirk, G.J., Repa, C., and LeDoux, J.E. (1995). Fear conditioning enhances short-latency auditory responses of lateral amygdala neurons: parallel recordings in the freely behaving rat. *Neuron* 15, 1029–1039. [https://doi.org/10.1016/0896-6273\(95\)90092-6](https://doi.org/10.1016/0896-6273(95)90092-6).
 24. Tsvetkov, E., Carlezon, W.A., Benes, F.M., Kandel, E.R., and Bolshakov, V.Y. (2002). Fear conditioning occludes LTP-induced presynaptic enhancement of synaptic transmission in the cortical pathway to the lateral amygdala. *Neuron* 34, 289–300. [https://doi.org/10.1016/s0896-6273\(02\)00645-1](https://doi.org/10.1016/s0896-6273(02)00645-1).
 25. Rumpel, S., LeDoux, J., Zador, A., and Malinow, R. (2005). Postsynaptic receptor trafficking underlying a form of associative learning. *Science* 308, 83–88. <https://doi.org/10.1126/science.1103944>.
 26. Scelfo, B., Sacchetti, B., and Strata, P. (2008). Learning-related long-term potentiation of inhibitory synapses in the cerebellar cortex. *Proc. Natl. Acad. Sci. USA* 105, 769–774. <https://doi.org/10.1073/pnas.0706342105>.
 27. Dubois, C.J., and Liu, S.J. (2021). GluN2D NMDA receptors gate fear extinction learning and interneuron plasticity. *Front. Synaptic Neurosci.* 13, 681068. <https://doi.org/10.3389/fnsyn.2021.681068>.
 28. Han, S., Soleiman, M.T., Soden, M.E., Zweifel, L.S., and Palmiter, R.D. (2015). Elucidating an affective pain circuit that creates a threat memory. *Cell* 162, 363–374. <https://doi.org/10.1016/j.cell.2015.05.057>.
 29. Chiang, M.C., Nguyen, E.K., Canto-Bustos, M., Papale, A.E., Oswald, A.M.M., and Ross, S.E. (2020). Divergent neural pathways emanating from the lateral parabrachial nucleus mediate distinct components of the pain response. *Neuron* 106, 927–939.e5. <https://doi.org/10.1016/j.neuron.2020.03.014>.
 30. Deng, J., Zhou, H., Lin, J.K., Shen, Z.X., Chen, W.Z., Wang, L.H., Li, Q., Mu, D., Wei, Y.C., Xu, X.H., and Sun, Y.G. (2020). The parabrachial nucleus directly channels spinal nociceptive signals to the intralaminar thalamic nuclei, but not the amygdala. *Neuron* 107, 909–923.e6. <https://doi.org/10.1016/j.neuron.2020.06.017>.
 31. Zhu, Y.-B., Wang, Y., Hua, X.-X., Xu, L., Liu, M.-Z., Zhang, R., Liu, P.-F., Li, J.-B., Zhang, L., and Mu, D. (2022). PBN-PVT projections modulate negative affective states in mice. *eLife* 11, e68372. <https://doi.org/10.7554/eLife.68372>.
 32. Ito, M., Nagase, M., Tohyama, S., Mikami, K., Kato, F., and Watabe, A.M. (2021). The parabrachial-to-amygdala pathway provides aversive information to induce avoidance behavior in mice. *Mol. Brain* 14, 94. <https://doi.org/10.1186/s13041-021-00807-5>.
 33. Campos, C.A., Bowen, A.J., Roman, C.W., and Palmiter, R.D. (2018). Encoding of danger by parabrachial CGRP neurons. *Nature* 555, 617–622. <https://doi.org/10.1038/nature25511>.
 34. Palmiter, R.D. (2018). The parabrachial nucleus: CGRP neurons function as a general alarm. *Trends Neurosci.* 41, 280–293. <https://doi.org/10.1016/j.tins.2018.03.007>.
 35. Sato, M., Ito, M., Nagase, M., Sugimura, Y.K., Takahashi, Y., Watabe, A.M., and Kato, F. (2015). The lateral parabrachial nucleus is actively involved in the acquisition of fear memory in mice. *Mol. Brain* 8, 22. <https://doi.org/10.1186/s13041-015-0108-z>.
 36. Zingg, B., Chou, X.L., Zhang, Z.G., Mesik, L., Liang, F., Tao, H.W., and Zhang, L.I. (2017). AAV-mediated anterograde transsynaptic tagging: mapping corticocollicular input-defined neural pathways for defense behaviors. *Neuron* 93, 33–47. <https://doi.org/10.1016/j.neuron.2016.11.045>.
 37. Snider, R.S., and Stowell, A. (1944). Receiving areas of the tactile, auditory, and visual systems in the cerebellum. *J. Neurophysiol.* 7, 331–357. <https://doi.org/10.1152/jn.1944.7.6.331>.
 38. Ressler, R.L., and Maren, S. (2019). Synaptic encoding of fear memories in the amygdala. *Curr. Opin. Neurobiol.* 54, 54–59. <https://doi.org/10.1016/j.conb.2018.08.012>.
 39. Roy, D.S., Park, Y.G., Kim, M.E., Zhang, Y., Ogawa, S.K., DiNapoli, N., Gu, X., Cho, J.H., Choi, H., Kamentsky, L., et al. (2022). Brain-wide mapping reveals that engrams for a single memory are distributed across multiple brain regions. *Nat. Commun.* 13, 1799. <https://doi.org/10.1038/s41467-022-29384-4>.
 40. Wheeler, A.L., Teixeira, C.M., Wang, A.H., Xiong, X., Kovacevic, N., Lerch, J.P., McIntosh, A.R., Parkinson, J., and Frankland, P.W. (2013). Identification of a functional connectome for long-term fear memory in mice. *PLoS Comput. Biol.* 9, e1002853. <https://doi.org/10.1371/journal.pcbi.1002853>.
 41. Chiang, M.C., Bowen, A., Schier, L.A., Tupone, D., Uddin, O., and Heinricher, M.M. (2019). Parabrachial complex: a hub for pain and aversion. *J. Neurosci.* 39, 8225–8230. <https://doi.org/10.1523/JNEUROSCI.1162-19.2019>.
 42. Missig, G., Mei, L., Vizzard, M.A., Braas, K.M., Waschek, J.A., Ressler, K.J., Hammack, S.E., and May, V. (2017). Parabrachial pituitary adenylate cyclase-activating polypeptide activation of amygdala endosomal extracellular signal-regulated kinase signaling regulates the emotional component of pain. *Biol. Psychiatry* 81, 671–682. <https://doi.org/10.1016/j.biopsych.2016.08.025>.
 43. Ressler, K.J., Mercer, K.B., Bradley, B., Jovanovic, T., Mahan, A., Kerley, K., Norrholm, S.D., Kilaru, V., Smith, A.K., Myers, A.J., et al. (2011). Post-traumatic stress disorder is associated with PACAP and the PAC1 receptor. *Nature* 470, 492–497. <https://doi.org/10.1038/nature09856>.
 44. Han, J.K., Kwon, S.H., Kim, Y.G., Choi, J., Kim, J.I., Lee, Y.S., Ye, S.K., and Kim, S.J. (2021). Ablation of STAT3 in Purkinje cells reorganizes cerebellar synaptic plasticity in long-term fear memory network. *eLife* 10, e63291. <https://doi.org/10.7554/eLife.63291>.
 45. ten Brinke, M.M., Heiney, S.A., Wang, X., Proietti-Onori, M., Boele, H.-J., Bakermans, J., Medina, J.F., Gao, Z., and De Zeeuw, C.I. (2017). Dynamic modulation of activity in cerebellar nuclei neurons during pavlovian eyeblink conditioning in mice. *eLife* 6, e28132. <https://doi.org/10.7554/eLife.28132>.
 46. Heffley, W., and Hull, C. (2019). Classical conditioning drives learned reward prediction signals in climbing fibers across the lateral cerebellum. *eLife* 8, e46764. <https://doi.org/10.7554/eLife.46764>.
 47. Onuki, Y., Van Someren, E.J.W., De Zeeuw, C.I., and Van der Werf, Y.D. (2015). Hippocampal-cerebellar interaction during spatio-temporal prediction. *Cereb. Cortex* 25, 313–321. <https://doi.org/10.1093/cercor/bht221>.
 48. Igloi, K., Doeller, C.F., Paradis, A.L., Benchenane, K., Berthoz, A., Burgess, N., and Rondi-Reig, L. (2015). Interaction between Hippocampus and cerebellum crus I in sequence-based but not place-based navigation. *Cereb. Cortex* 25, 4146–4154. <https://doi.org/10.1093/cercor/bhu132>.
 49. Phillips, R.G., and LeDoux, J.E. (1992). Differential contribution of amygdala and hippocampus to cued and contextual fear conditioning. *Behav. Neurosci.* 106, 274–285. <https://doi.org/10.1037/0735-7044.106.2.274>.
 50. Supple, W.F., Jr., Cranney, J., and Leaton, R.N. (1988). Effects of lesions of the cerebellar vermis on VMH lesion-induced hyperdefensiveness,

- spontaneous mouse killing, and freezing in rats. *Physiol. Behav.* 42, 145–153. [https://doi.org/10.1016/0031-9384\(88\)90290-9](https://doi.org/10.1016/0031-9384(88)90290-9).
51. Barsy, B., Kocsis, K., Magyar, A., Babiczky, Á., Szabó, M., Veres, J.M., Hillier, D., Ulbert, I., Yizhar, O., and Mátýás, F. (2020). Associative and plastic thalamic signaling to the lateral amygdala controls fear behavior. *Nat. Neurosci.* 23, 625–637. <https://doi.org/10.1038/s41593-020-0620-z>.
 52. Maren, S., and Quirk, G.J. (2004). Neuronal signalling of fear memory. *Nat. Rev. Neurosci.* 5, 844–852. <https://doi.org/10.1038/nrn1535>.
 53. LeDoux, J.E., Farb, C., and Ruggiero, D.A. (1990). Topographic organization of neurons in the acoustic thalamus that project to the amygdala. *J. Neurosci.* 10, 1043–1054. <https://doi.org/10.1523/jneurosci.10-04-01043.1990>.
 54. Aitkin, L.M., and Boyd, J. (1978). Acoustic input to the lateral pontine nuclei. *Hear. Res.* 1, 67–77. [https://doi.org/10.1016/0378-5955\(78\)90010-2](https://doi.org/10.1016/0378-5955(78)90010-2).
 55. Huffman, R.F., and Henson, O.W. (1990). The descending auditory pathway and acousticomotor systems: connections with the inferior colliculus. *Brain Res. Brain Res. Rev.* 15, 295–323. [https://doi.org/10.1016/0165-0173\(90\)90005-9](https://doi.org/10.1016/0165-0173(90)90005-9).
 56. McCormick, D.A., and Thompson, R.F. (1984). Neuronal responses of the rabbit cerebellum during acquisition and performance of a classically conditioned nictitating membrane-eyelid response. *J. Neurosci.* 4, 2811–2822. <https://doi.org/10.1523/JNEUROSCI.04-11-02811.1984>.
 57. Freeman, J.H., and Steinmetz, A.B. (2011). Neural circuitry and plasticity mechanisms underlying delay eyeblink conditioning. *Learn. Mem.* 18, 666–677. <https://doi.org/10.1101/lm.2023011>.
 58. Koutsikou, S., Crook, J.J., Earl, E.V., Leith, J.L., Watson, T.C., Lumb, B.M., and Apps, R. (2014). Neural substrates underlying fear-evoked freezing: the periaqueductal grey-cerebellar link. *J. Physiol.* 592, 2197–2213. <https://doi.org/10.1113/jphysiol.2013.268714>.
 59. Kebschull, J.M., Richman, E.B., Ringach, N., Friedmann, D., Albaran, E., Kolluru, S.S., Jones, R.C., Allen, W.E., Wang, Y., Cho, S.W., et al. (2020). Cerebellar nuclei evolved by repeatedly duplicating a conserved cell-type set. *Science* 370, eabd5059. <https://doi.org/10.1126/science.abd5059>.
 60. De Bellis, M.D., and Kuchibhatla, M. (2006). Cerebellar volumes in pediatric maltreatment-related posttraumatic stress disorder. *Biol. Psychiatry* 60, 697–703. <https://doi.org/10.1016/j.biopsych.2006.04.035>.
 61. Ohyama, T., Nores, W.L., Medina, J.F., Riusech, F.A., and Mauk, M.D. (2006). Learning-induced plasticity in deep cerebellar nucleus. *J. Neurosci.* 26, 12656–12663. <https://doi.org/10.1523/jneurosci.4023-06.2006>.
 62. Wang, X., Yu, S.-y., Ren, Z., De Zeeuw, C.I., and Gao, Z. (2020). A FN-MdV pathway and its role in cerebellar multimodular control of sensorimotor behavior. *Nat. Commun.* 11, 6050. <https://doi.org/10.1038/s41467-020-19960-x>.
 63. Luis-Islas, J., Luna, M., Floran, B., and Gutierrez, R. (2022). Optoception: perception of optogenetic brain perturbations. *eNeuro* 9, ENEURO.0216-0222.2022. <https://doi.org/10.1523/ENEURO.0216-22.2022>.
 64. Schneider, C.A., Rasband, W.S., and Eliceiri, K.W. (2012). NIH Image to ImageJ: 25 years of image analysis. *Nat. Methods* 9, 671–675. <https://doi.org/10.1038/nmeth.2089>.
 65. Shamash, P., Carandini, M., Harris, K., and Steinmetz, N. (2018). A tool for analyzing electrode tracks from slice histology. Preprint at bioRxiv. <https://doi.org/10.1101/447995>.
 66. Cummings, K.A., Bayshmak, S., Dong, T.N., Kenny, P.J., and Clem, R.L. (2022). Control of fear by discrete prefrontal GABAergic populations encoding valence-specific information. *Neuron* 110, 3036–3052.e5. <https://doi.org/10.1016/j.neuron.2022.07.004>.
 67. Chaplan, S.R., Bach, F.W., Pogrel, J.W., Chung, J.M., and Yaksh, T.L. (1994). Quantitative assessment of tactile allodynia in the rat paw. *J. Neurosci. Methods* 53, 55–63. [https://doi.org/10.1016/0165-0270\(94\)90144-9](https://doi.org/10.1016/0165-0270(94)90144-9).

STAR★METHODS

KEY RESOURCES TABLE

REAGENT or RESOURCE	SOURCE	IDENTIFIER
Antibodies		
Rabbit monoclonal anti-c-Fos (9F6)	Cell Signaling Technology	Cat# 2250; RRID: AB_2247211
Rabbit polyclonal anti-PACAP-38	Peninsula Laboratories	Cat# T-4473; RRID: AB_519166
Sheep polyclonal anti-FoxP2	R&D Systems	Cat# AF5647; RRID: AB_2107133
Mouse monoclonal anti-CGRP	Abcam	Cat# ab81887; RRID: AB_1658411
Alexa Fluor 568-conjugated donkey anti-mouse	Invitrogen	Cat# A10037; RRID: AB_2534013
Alexa Fluor 594-conjugated donkey anti-sheep	Abcam	Cat# ab150180; RRID: AB_2716768
Alexa Fluor 568-conjugated goat anti-rabbit	Invitrogen	Cat# A11011; RRID: AB_143157
Alexa Fluor 647-conjugated donkey anti-rabbit	Invitrogen	Cat# A31573; RRID: AB_2536183
Bacterial and virus strains		
AAV-EF1α-DIO-EYFP	Addgene	Cat# 27056-AAV1; RRID: Addgene_27056
AAV-EF1α-DIO-eNpHR3.0-EYFP	Addgene	Cat# 26966-AAV1; RRID: Addgene_26966
AAV-EF1α-double floxed-hChR2(H134R)-EYFP-WPRE-HGHpA	Addgene	Cat# 20298-AAV1; RRID: Addgene_20298
AAVrg-EF1α-mCherry-IRES-Cre	Addgene	Cat# 55632-AAVrg; RRID: Addgene_55632
AAV-hSyn-double floxed-hChR2(H134R)-EYFP	Addgene	Cat# 26973-AAV1; RRID: Addgene_26973
AAV-hSyn-eNpHR3.0-EYFP	Addgene	Cat# 26972-AAV5; RRID: Addgene_26972
AAV-CAG-FLEX-GCaMP6s-WPRE-SV40	Addgene	Cat# 100842-AAV1; RRID: Addgene_100842
AAVrg-hSyn-EGFP	Addgene	Cat# 50465-AAVrg; RRID: Addgene_50465
AAV-hSyn-EGFP	Addgene	Cat# 50465-AAV5; RRID: Addgene_50465
pENN-AAV-hSyn-Cre-WPRE-hGH	Addgene	Cat# 105553-AAV1; RRID: Addgene_105553
AAV-hSyn-FLEX-mGFP-2A-Synaptophysin-mRuby	Addgene	Cat# 71760-AAV1; RRID: Addgene_71760
rAAV8-CAG-mCherry-IRES-WGA-Cre	UNC vector Core	Cat# AV5901FG
Chemicals, peptides, and recombinant proteins		
Normal Donkey Serum	Sigma	Cat# D9663
Triton X-100	Sigma	Cat# X100
DAPI mounting solution	Vectorlab	Cat# H-1200
Retrobead (red)	LumaFluor	N/A

(Continued on next page)

Continued

REAGENT or RESOURCE	SOURCE	IDENTIFIER
Experimental models: Organisms/strains		
C57BL/6NCrlOri	Orient Bio	N/A
Software and algorithms		
GraphPad Prism	GraphPad	RRID:SCR_002798
ImageJ	(Schneider et al.) ⁶⁴	https://imagej.nih.gov/ij/
MATLAB	MathWorks	RRID:SCR_001622
Zen	ZEISS	RRID:SCR_013672
Ethovision XT 14	Noldus	RRID:SCR_000441
Synapse	Tucker-Davis Technologies	N/A
Patchmaster	HEKA	RRID:SCR_000034
Igor Pro	Wave Metrics	RRID:SCR_000325
Mini Analysis	Synaptosoft	RRID:SCR_002184
Other		
Fiber Optic Cannula	RWD	Cat# R-FOC-L400C-39NA Cat# R-FOC-L200C-39NA
Slide Scanner ZEISS Axio Scan.Z1	ZEISS	N/A
Slide Scanner	OLYMPUS	Cat# VS200
Confocal microscope	OLYMPUS	Cat# FV3000
MATLAB codes for brain ROI mapping	(Shamash et al.) ⁶⁵	https://github.com/cortex-lab/allenCCF
MATLAB codes for Fiber photometry analysis	Tucker-Davis Technologies	https://www.tdt.com/docs/sdk/offline-data-analysis/offline-data-matlab/licking-bout-e poc-filtering/

RESOURCE AVAILABILITY

Lead contact

Additional information and requests for resources and reagents should be directed to and will be fulfilled by the lead contact, Yong-Seok Lee (yongseok7@snu.ac.kr).

Materials availability

This study did not generate new unique reagents.

Data and code availability

- All data that support the findings of this study are available from the [lead contact](#) upon request.
- This paper does not report original code.
- Any additional information required to reanalyze the data reported in this paper is available from the [lead contact](#) upon request.

EXPERIMENTAL MODEL AND SUBJECT DETAILS

Animals

Male wild type mice (C57Bl/6NCrlOri, 5–10 weeks of age) were purchased from Orient Bio Inc (Korea). Mice were group-housed (4 mice per cage) on a 12-h light/dark cycle in vivarium at SNU. Food and water were available *ad libitum*. Mice were used for experiments after a minimum of 7 days of habituation in the animal facility. All experiments were performed in accordance with the guidelines approved by the Institutional Animal Care and Use Committee of Seoul National University (SNU-181122-5-3).

METHOD DETAILS

Stereotaxic surgeries

Mice were anesthetized using intraperitoneal injection of a zoletil/rompun mixture (30 mg/kg and 10 mg/kg, respectively) and were fixed on a stereotaxic apparatus (Kopf instruments). A volume of 300–400 nL of AAVs or retrobeads was injected into the lateral parabrachial nucleus (IPBN) and deep cerebellar nuclei (DCN) using a 30-gauge syringe (Hamilton). The coordinates used for viral

injections were as follows: IPBN, −4.7 mm anteroposterior (AP) from bregma, ±1.2 mm mediolateral (ML) from bregma, −3.8 mm dorsoventral (DV) from the skull; DCN, −6.3 mm AP from bregma, ±1.2 mm ML from bregma, −3.2 mm DV from the skull surface. The coordinates used for optic fiber implantations were as follows: IPBN, −4.7 mm AP from bregma, ±1.2 mm ML from bregma, −3.6 mm DV from the skull for optogenetic manipulation, −3.7 mm DV from the skull for fiber photometry recordings; DCN, −6.3 mm AP from bregma, ±1.2 mm ML from bregma, −3.0 mm DV from the skull for optogenetic manipulations and −3.1 mm DV from the skull for fiber photometry recordings. Optic cannulas (200 μm in diameter, 0.39 NA, RWD) were bilaterally implanted for optogenetic manipulation. Optic cannulas (400 μm in diameter, 0.39 NA) were unilaterally implanted for fiber photometry recordings.

For validation of DCN output targets, AAV5-hSyn-EGFP (3.0×10^{12} copies per mL) was injected into the DCN. For validation of DCN-connected IPBN output targets, rAAV8-EF1α-mCherry-IRES-WGA-Cre (1.4×10^{12} copies per mL) and AAV1-EF1α-DIO-EYFP (5.0×10^{12} copies per mL) were injected into the DCN and the IPBN, respectively. Alternatively, pENN-AAV1-hSyn-Cre-WPRE-hGH (4.0×10^{12} copies per mL) and AAV1-hSyn-FLEX-mGFP-2A-Synaptophysin-mRuby (3.0×10^{12} copies per mL) were injected into the DCN and the IPBN, respectively. For optogenetic inhibition of IPBN-projecting DCN neurons, AAV1-EF1α-DIO-eNpHR3.0-EYFP (5.0×10^{12} copies per mL) and AAV-retrograde-EF1α-mCherry-IRES-Cre (3.0×10^{12} copies per mL) were injected into the DCN and the IPBN, respectively, with optic cannula implantation targeting the DCN. For optogenetic activation of IPBN-projecting DCN neurons, AAV1-EF1α-double floxed-hChR2(H134R)-EYFP-WPRE-HGHpA (5.0×10^{12} copies per mL) and AAV-retrograde-EF1α-mCherry-IRES-Cre (3.0×10^{12} copies per mL) were injected into the DCN and the IPBN, respectively, with optic cannula implantation targeting the DCN. For ex-vivo slice recording in DCN-connected IPBN neurons, AAV1-EF1α-double floxed-hChR2(H134R)-EYFP-WPRE-HGHpA (5.0×10^{12} copies per mL) and AAV-retrograde-EF1α-mCherry-IRES-Cre (3.0×10^{12} copies per mL) were injected into the DCN and the IPBN, respectively. For fiber photometry recording in DCN-connected IPBN neurons, rAAV8-EF1α-mCherry-IRES-WGA-Cre (1.4×10^{12} copies per mL) and AAV1-CAG-FLEX-GCaMP6s-WPRE-SV40 (1.0×10^{13} copies per mL) were injected into the DCN and IPBN, respectively with optic cannula implantation targeting the IPBN. For c-Fos immunohistochemistry in IPBN-projecting DCN neurons, AAV-retrograde-hSyn-EGFP (3.0×10^{12} copies per mL) was injected into the IPBN. For retrograde tracing of the DCN-IPBN circuit, retrobeads were injected into the IPBN. For optogenetic inhibition of DCN terminals targeting the IPBN, AAV5-hSyn-eNpHR3.0-EYFP (5.0×10^{12} copies per mL) was injected into the DCN with optic cannula implantation targeting the IPBN. For optogenetic activation of DCN-connected IPBN neurons, AAV1-hSyn-hChR2(H134R)-EYFP (5.0×10^{12} copies per mL) was injected into the DCN with optic cannula implantation targeting the IPBN. We only included the data of mice which has IPBN- or DCN-specific viral expression and accurate targeting of optic fibers to the DCN without severe damage in the DCN.

Fear conditioning and optogenetic manipulation

At 3 weeks after stereotaxic injection and fiber optic cannula implantation, mice were handled for at least 4 days, followed by habituation to patchcord connection for at least 3 min per day for 2 days. For experiments to inhibit the DCN-IPBN pathway during fear learning, on day 1, mice were connected to a patchcord and received five pairs of an electrical footshock (0.5 mA, 1 s), tone (80 dB, 2800 Hz, 30 s), and constant yellow laser delivery (593.5 nm, 10 mW, 30 s) which were co-terminated in the fear conditioning chamber (Coulbourn Instruments, context A). On day 2, mice were placed in a novel context (cylinder chamber, context B) and received the same tone (80 dB, 2800 Hz, 30 s) twice with a 30-s interval without the yellow laser. On day 3, mice were re-exposed to the fear conditioning chamber without the patchcord connected.

For experiments to inhibit the DCN-IPBN pathway during fear memory retrieval using NpHR, on day 1, mice were placed in a fear conditioning chamber and received five pairs of an electrical footshock (0.5 mA, 1 s) and tone (80 dB, 2800 Hz, 30 s) which were co-terminated. On day 2, mice were connected to the patchcord and were placed in context B. After 3 min, mice received the same tone (80 dB, 2800 Hz, 30 s) paired with constant yellow laser delivery (593.5 nm, 10 mW, 30 s) twice with a 30-s interval. On day 3, mice were connected to the patchcord and were re-exposed to context A with constant yellow light delivery (593.5 nm, 10 mW) for 2 min. For optogenetic inhibition of DCN-connected IPBN neurons, mice were placed in context A for 30 s.

For experiments using ChR2 to stimulate the DCN-IPBN circuit to measure behavioral effects, on day 1, mice were connected to a patchcord and were placed in another context (context C) where they received three trains of 30-s blue light delivery (473 nm, 20 Hz, 20-ms pulses, 8–10 mW) with 30-s intervals. On day 2, mice were re-exposed to the same chamber (context C) for 2 min without the patchcord connected. On day 3, mice were placed in the fear conditioning chamber (context A) without the patchcord connected and received five pairs of an electrical footshock (0.5 mA, 2 s) and tone (80 dB, 2800 Hz, 30 s) which were co-terminated. On day 4, mice were placed in a cylinder chamber (context B) and received 30-s blue light delivery (473 nm, 20 Hz, 20-ms pulses, 8–10 mW), same tone (80 dB, 2800 Hz, 30 s) and a pairing of the 30-s blue light delivery and same tone in series.

For experiments to stimulate the DCN-IPBN circuit paired with footshocks for fear conditioning, on day 1, mice received five pairings of 30-s blue light delivery (473 nm, 20 Hz, 20-ms pulses, 8–10 mW) and footshock stimulus (0.5 mA, 2 s) which were co-terminated with 30-s intervals. On day 2, mice were placed in context B and received 30-s blue light delivery. On day 3, mice were placed in context A to test contextual fear memory.

For experiments to stimulate the DCN-IPBN circuit paired with auditory tones for fear conditioning, on day 1, mice received five pairings of 30-s blue light delivery (473 nm, 20 Hz, 20-ms pulses, 8–10 mW) and auditory stimulus (2800 Hz, 80 dB, 30 s) which were co-terminated with 30-s intervals. On day 2, mice were placed in context B and received the auditory stimulus.

For unpaired fear conditioning, mice received auditory stimulus five times with 30-s intervals in the context A and were returned to the home cage. 15 min later, they were placed in the same chamber and received the electrical shock five times with 1-min intervals on day 1.⁶⁶ On day 2, the mice were placed in the context B and received the same auditory stimuli. Mice were considered to exhibit freezing behavior if they did not demonstrate any movement except for breathing for at least 3 s. Freezing behavior in mice was analyzed manually. The experimenters were blinded to experimental conditions.

Fox urine exposure

Mice were placed in a small chamber containing twice-folded KimWipes laboratory tissues treated with 20 µL of 20% trimethylthiazoline (TMT), which is a component of fox urine, for 10 min paired with constant yellow laser delivery (593.5 nm, 10 mW, 10 min). Freezing behavior was scored manually.

Von frey test

Mice were placed in a transparent circular on a grid mesh floor table and allowed to habituate for 30 min with yellow laser delivery. Hindpaws were stimulated with a set of von Frey filaments (0.16, 0.4, 0.6, 1, and 1.4 g) with yellow laser delivery. The withdrawal threshold of 1.5 g was used as a cut-off. Paw withdrawal thresholds were evaluated using the up-down method.⁶⁷

Social interaction

For social habituation in a white opaque acrylic three-chambered apparatus with two doors between the chambers (40 cm × 60 cm size, each chamber 20-cm wide), mice were allowed to explore the three-chambered apparatus during 15 min. After 2 days of habituation to the apparatus, mice were allowed to explore a novel mouse and a novel object in the same apparatus with constant yellow laser delivery for 10 min. Time spent exploring the mouse or the object was scored manually.

Open field test

Mice were placed in a white opaque acrylic box (40 cm × 40 cm × 50 cm) and allowed to move freely in the chamber for 12 min with constant yellow laser delivery (593.5 nm, 10 mW) throughout the test session. Locomotor activity was analyzed using Ethovision 14 software (Noldus).

Fiber photometry

To label DCN-connected IPBN neurons with GCaMP6s, mice were injected with 300–400 nL per site of retrograde AAV-mCherry-IRES-Cre targeting the IPBN (AP: −4.7 mm from bregma, ML: ±1.2 mm from bregma, DV: −3.8 mm from the skull) and with 300–400 nL per site of AAV1-CAG-DIO-GCaMP6s targeting the DCN (AP: −6.3 mm from bregma, ML: +1.2 mm from bregma, DV: −3.1 mm from the skull). A single 400-µm fiber-optic (RWD, R-FOC-L400C, 0.5 NA) was implanted into the IPBN (AP: −4.7 mm from bregma, ML: +1.2 mm from bregma, DV: −3.7 mm from the skull) for recordings.

Two excitation lights from 465 nm to 405 nm LEDs (Doric Lenses) were sinusoidally modulated by a real-time processor (RZ5P, Tucker Davis Technologies) at 211 and 531 Hz, respectively. The light intensity was maintained at 0.1–0.2 mW during all recordings. The fluorescence signal was focused onto a fluorescence detector amplifier (Doric Lenses). The resulting signals were demodulated, amplified, and collected at approximately 1 kHz by the TDT RZ5P processor and TDT synapse software. The signals were down-sampled to 2 Hz, and the resulting ΔF/F was calculated as (raw 465-nm signal – fitted 405-nm signal)/(fitted 405-nm signal) using MATLAB codes provided by <https://www.tdt.com/docs/sdk/offline-data-analysis/offline-data-matlab>. The fluorescence signals were aligned by TTL output signals which were co-triggered with the onset of tone or shock delivery from the fear conditioning set-up to the real-time processor for fiber photometry recording.

Electrophysiology

For measurement of optogenetically induced responses in the DCN-PBN pathway, young adult (5–8 weeks of age) male mice were injected with 300–400 nL of AAV1-EF1α-DIO-ChR2(H134R)-EYFP targeting the DCN (AP: −6.3 mm from bregma, ML: +1.2 mm from bregma, DV: −3.1 mm from the skull) and with 300–400 nL per site of retrograde AAV-mCherry-IRES-Cre targeting the PBN (AP: −4.7 mm from bregma, ML: ±1.2 mm from bregma, DV: −3.8 mm from the skull). After 3 weeks, mice were euthanized with isoflurane and transcardially perfused with an ice-cold cutting solution containing the following (in mM): 2.5 KCl, 30 NaHCO₃, 93 NMDG, 20 HEPES, 2 thiourea, 1.25 NaH₂PO₄, 10 MgSO₄, 24 D-glucose, 5 sodium ascorbate, 3 sodium pyruvate and 0.5 CaCl₂. The brain was removed and placed into the ice-cold cutting solution, which was saturated with 95% O₂/5% CO₂ for at least 30 min before use. After acute slice preparation (300-µm coronal sections; Leica, VT1000S), slices were incubated in the cutting solution for 10 min at 32°C. Slices were then transferred to artificial cerebrospinal fluid (ACSF) containing the following (in mM): 125 NaCl, 2.5 KCl, 1 MgCl₂, 2 CaCl₂, 1.25 NaH₂PO₄, 26 NaHCO₃, 10 glucose. Slices were incubated for at least 1 h at room temperature until use. Slices were transferred to a recording chamber perfused with ACSF at a rate of 4 mL/min and maintained at 32°C.

Whole-cell recordings were performed using EPC 10 amplifier (HEKA Electronik) with a sampling frequency of 20 kHz, and signals were filtered at 10 kHz. Patch pipettes (3–4 MΩ) were filled with internal solution containing the following (in mM): 9 KCl, 10 KOH, 120 K-gluconate, 3.48 MgCl₂, 10 HEPES, 4 NaCl, 4 Na₂ATP, 0.4 Na₃GTP, and 17.5 sucrose (pH 7.25). The membrane potential was held at −70 mV in voltage-clamped and current-clamped recordings. In voltage-clamped recording, cerebellar axons in coronal slices

containing the PBN were activated using a 473 nm laser (5 ms, 5 mW at the fiber tip, Laserglow Technologies) coupled with an opto-patcher (A-M SYSTEMS). We found that 5 mW is the minimal laser intensity for inducing maximal synaptic responses at the DCN-IPBN synapse in naive mice and determined to use 5 mW (5 ms) for all the optogenetically-induced excitatory synaptic current (oEPSC) measurements. oEPSC responses were evoked by paired laser pulses with a 100-ms interval. 5 sweeps of laser stimulation were delivered with 20-s intervals and 5 oEPSC responses in the same neuron were averaged. 3 min after observing oEPSC, spontaneous EPSC was recorded for 100 s. In current-clamped recording, we measured resting membrane potential, firing frequency of action potentials by current injections (50–300 pA, 50 pA steps), and input resistances by injecting hyperpolarization current (−50 pA). For ex vivo slice recordings in the PBN, mice were trained with a fear conditioning paradigm: 1) tone and shock pairing, 2) only shock delivered, 3) home cage (control). Mice were sacrificed for slice recordings 24 h later.

To measure AMPA/NMDA ratios in DCN-connected IPBN neurons, patch pipettes (3–4 MΩ) were filled with internal solution containing the following (in mM): 135 mM CsMS; 10 mM CsCl; 10 mM HEPES; 0.2 mM EGTA; 4 mM Mg-ATP; 0.4 mM Na₂-GTP; 0.5 mM spermine; ~ 295 mOsm; pH 7.3 adjusted with CsOH. The membrane potential was held at −70 mV and +40 mV in VC mode to measure AMPAR- and NMDAR-mediated oEPSCs, respectively, with 100 μM picrotoxin-containing ACSF. NMDAR-mediated responses were measured 50 ms after the onset of optogenetic stimulation. AMPA/NMDA ratios were calculated by dividing the peak amplitudes. Spontaneous EPSCs were analyzed using Mini Analysis Program (Synaptosoft) and other all experimental data were analyzed using Igor Pro (Wave Metrics). Experimenter performing electrophysiology experiments was blinded to the group information.

Tissue fixation and sectioning

Mice were perfused with phosphate-buffered saline (PBS), followed by 4% paraformaldehyde (PFA). Brains were dissected, post-fixed in 4% PFA overnight at 4°C, then transferred to a 30% (w/v) sucrose solution and stored for 48 h at 4°C. Brains were sectioned into 30-μm coronal sections covering the full anterior-posterior extent of the PBN and DCN.

Histology

For immunohistochemistry, sections were washed three times in PBS for 10 min and incubated in blocking solution (3% normal donkey serum and 0.1% Triton X-100 in PBS) for 1 h at room temperature. The sections were incubated overnight or for 48 h (c-Fos) at 4°C in blocking solution with primary antibodies including: anti-mouse CGRP (1:1000, Abcam, ab81887), anti-rabbit PACAP (1:1000, Peninsula Laboratories, T-4473), anti-sheep FOXP2 (1:1000, R&D Systems, AF5647), and anti-c-Fos (1:1000, Cell Signaling) primary antibodies. The sections were washed three times in PBS for 10 min and incubated for 3 h or 24 h (c-Fos) in blocking solution with secondary antibodies including: Alexa Fluor 568 donkey anti-mouse (1:500, Invitrogen, A10037), Alexa Fluor 594 donkey anti-sheep (1:500, Abcam, ab150180), Alexa Fluor 568 goat anti-rabbit (1:500, Invitrogen, A11011), and Alexa Fluor 647 donkey anti-rabbit (1:400, Invitrogen, A-31573) secondary antibodies. The sections were washed three times in PBS for 10 min, mounted onto glass slides, and cover-slipped with mounting solution containing DAPI (Vectorlab, H-1200). Fluorescent images were acquired using a confocal microscope (Olympus, FV-3000) or slide scanners (Zeiss, Axio Scan Z1 or Olympus, VS200). For region of interest (ROI) mapping with DCN and IPBN projection data, we used a MATLAB-based software provided by <https://github.com/cortex-lab/allenCCF>⁶⁶ and ImageJ.⁶⁴

QUANTIFICATION AND STATISTICAL ANALYSIS

Data are presented as mean ± SEM for all experiments. Statistical analyses were performed using GraphPad Prism 7 software. When comparing two populations of data, two-tailed unpaired t test, two-tailed paired t test, two-tailed Mann Whitney t test were used. When comparing multiple populations of data, one-way or two-way analysis of variance (ANOVA) followed by Tukey or Bonferroni post-hoc tests was used. All statistical data can be found in the figure legends. All N values for the number of cells or animals are reported in the figure legends. Statistical significance was set at *p < 0.05, **p < 0.01, ***p < 0.001, ****p < 0.0001.